81 p.

NASA TN D-1983

NASA TN D-1983

N63 16746

TECHNICAL NOTE

D-1983

EXPERIMENTAL AND THEORETICAL STUDIES ON THE FORMATION OF DETONATION WAVES IN VARIABLE GEOMETRY TUBES

By

Loren E. Bollinger, Michael C. Fong,
James A. Laughrey, and Rudolph Edse

Prepared under Grant NsG-44-60 by
OHIO STATE UNIVERSITY
Columbus, Ohio
for

NATIONAL AERONAUTICS AND SPACE ADMINISTRATION

WASHINGTON June 1963

Note/

TABLE OF CONTENTS

	Page
SUMMARY	1
EXPERIMENTAL INVESTIGATION	2
A. Introduction	2
B. Experimental Equipment	4
C. Tube Geometry	5
D. Experimental Procedure	6
E. Results	7
F. Discussion	12
THEORETICAL INVESTIGATION	13
A. Introduction	13
Symbols	15
B. Interaction Between a Subsonic Flame and a Cross-Sectional Area Change	16
C. Interaction Between a Subsonic Flame and a Uniform Rod-Insert in a Constant-Area Duct	23
D. Empirical Relations	25
E. Discussion	26
CONCLUSIONS	29
REFERENCES	31

TABLE

1	Detonation Induction Distances for Cylindrical Rod Inserts	33
2	Comparison of Detonation Induction Distances for Hydrogen-Oxygen Mixtures in Cylindrical Tubes of Different Diameter	34
3	Detonation Induction Distances for the Diverging Insert	35
4	Detonation Induction Distances for the Right Angle Section Configuration	36
5	Evaluation of $(K)^{\frac{1}{4}}$ and $(\frac{L}{d})^{\frac{1}{4}}$ for Various Hydrogen-Oxygen Mixtures (d = 1.5 cm)	37
6	Evaluation of $(K)^{\frac{1}{4}}$ and $(\frac{L}{d})^{\frac{1}{4}}$ for Various Hydrogen-Oxygen Mixtures (d = 5.0 cm)	38
7	Evaluation of $(K)^{\frac{1}{4}}$ and $(\frac{L}{d})^{\frac{1}{4}}$ for Various Hydrogen-Oxygen Mixtures (d = 7.9 cm)	39

Page

TABLE

8 Evaluation of $(K)^{\frac{1}{4}}$ and $(\frac{L}{d})^{\frac{1}{4}}$ for Various Carbon Monoxide - Oxygen Mixtures (d = 1.5 cm) 40

FIGURE

1 Photograph of Detonation Tube 41
2 Exploded View of 79-mm Detonation Tube Section 42
3 Photograph of Flow Control System 43
4 Exploded View of Probe Assembly 44
5 Photograph of Chronograph System 45
6 Descriptive View of Cylindrical Insert, Diameter = 0.635 cm 46
7 Descriptive View of Cylindrical Insert, Diameter = 1.588 cm 47
8 Descriptive View of Cylindrical Insert, Diameter = 4.763 cm 48
9 Descriptive View of Divergent Stepped-Wall Insert 49
10 Right-Angle Section for Detonation Tube 50
11 Rate of Flame Propagation in H_2 - O_2 Mixture; Mole % H_2 = 45, p_i = 1 atm, t_i = 40° C, Clear Tube 51
12 Rate of Flame Propagation in H_2 - O_2 Mixture; Mole % H_2 = 66.67, p_i = 1 atm, t_i = 40° C, Clear Tube 51
13 Rate of Flame Propagation in H_2 - O_2 Mixture; Mole % H_2 = 75, p_i = 1 atm, t_i = 40° C, Clear Tube 52
14 Rate of Flame Propagation in H_2 - O_2 Mixture; Mole % H_2 = 45, p_i = 5 atm, t_i = 40° C, Clear Tube 52
15 Rate of Flame Propagation in H_2 - O_2 Mixture; Mole % H_2 = 66.67, p_i = 5 atm, t_i = 40° C, Clear Tube 53
16 Rate of Flame Propagation in H_2 - O_2 Mixture; Mole % H_2 = 75, p_i = 5 atm, t_i = 40° C, Clear Tube 53
17 Rate of Flame Propagation in H_2 - O_2 Mixture; Mole % H_2 = 66.67, p_i = 1 atm, t_i = 40° C, 0.635-cm diameter insert 54

Page

FIGURE

18 Rate of Flame Propagation in H_2 - O_2 Mixture; Mole % H_2 = 66.67, p_i = 5 atm, t_i = 40° C, 0.635-cm Diameter Insert 54

19 Rate of Flame Propagation in H_2 - O_2 Mixture; Mole % H_2 = 66.67, p_i = 1 atm, t_i = 40° C, 1.588-cm Diameter Insert 55

20 Rate of Flame Propagation in H_2 - O_2 Mixture; Mole % H_2 = 66.67, p_i = 5 atm, t_i = 40° C, 1.588-cm Diameter Insert 55

21 Rate of Flame Propagation in H_2 - O_2 Mixture; Mole % H_2 = 45, p_i = 1 atm, t_i = 40° C, 4.763-cm Diameter Insert 56

22 Rate of Flame Propagation in H_2 - O_2 Mixture; Mole % H_2 = 66.67, p_i = 1 atm, t_i = 40° C, 4.763-cm Diameter Insert 56

23 Rate of Flame Propagation in H_2 - O_2 Mixture; Mole % H_2 = 75, p_i = 1 atm, t_i = 40° C, 4.763-cm Diameter Insert 57

24 Rate of Flame Propagation in H_2 - O_2 Mixture; Mole % H_2 = 45, p_i = 5 atm, t_i = 40° C, 4.763-cm Diameter Insert 57

25 Rate of Flame Propagation in H_2 - O_2 Mixture; Mole % H_2 = 66.67, p_i = 5 atm, t_i = 40° C, 4.763-cm Diameter Insert 58

26 Rate of Flame Propagation in H_2 - O_2 Mixture; Mole % H_2 = 75, p_i = 5 atm, t_i = 40° C, 4.763-cm Diameter Insert 58

27 Detonation Induction Distances of Hydrogen-Oxygen Mixtures Based on Maximum Flame Propagation Rates for the Clear Tube and 0.635, 1.588, and 4.763-cm Diameter Inserts 59

28 Detonation Induction Distances of Hydrogen-Oxygen Mixtures Based on Average Flame Propagation Rates for the Clear Tube and 0.635, 1.588, and 4.763-cm Diameter Inserts 60

29 Rate of Flame Propagation in H_2 - O_2 Mixture; Mole % H_2 = 45, p_i = 1 atm, t_i = 40° C, Divergent Stepped-Wall Insert 61

Page

FIGURE

30 Rate of Flame Propagation in H_2 - O_2 Mixture; Mole % H_2 = 66.67, p_i = 1 atm, t_i = 40° C, Divergent Stepped-Wall Insert 61

31 Rate of Flame Propagation in H_2 - O_2 Mixture; Mole % H_2 = 75, p_i = 1 atm, t_i = 40° C, Divergent Stepped-Wall Insert 62

32 Detonation Induction Distances of H_2 - O_2 Mixtures Based on Maximum Flame Propagation Rates with a Divergent Stepped-Wall Insert 63

33 Detonation Induction Distances of H_2 - O_2 Mixtures Based on Average Flame Propagation Rates with a Divergent Stepped-Wall Insert 64

34 Rate of Flame Propagation in H_2 - O_2 Mixture; Mole % H_2 = 45, p_i = 1 atm, t_i = 40° C, 90°-Bend 66 cm From Ignitor 65

35 Rate of Flame Propagation in H_2 - O_2 Mixture; Mole % H_2 = 66.67, p_i = 1 atm, t_i = 40° C, 90°-Bend 66 cm From Ignitor 66

36 Rate of Flame Propagation in H_2 - O_2 Mixture; Mole % H_2 = 75, p_i = 1 atm, t_i = 40° C, 90°-Bend 66 cm From Ignitor 66

37 Rate of Flame Propagation in H_2 - O_2 Mixture; Mole % H_2 = 45, p_i = 5 atm, t_i = 40° C, 90°-Bend 66 cm From Ignitor 67

38 Rate of Flame Propagation in H_2 - O_2 Mixture; Mole % H_2 = 66.67, p_i = 5 atm, t_i = 40° C, 90°-Bend 66 cm From Ignitor 67

39 Rate of Flame Propagation in H_2 - O_2 Mixture; Mole % H_2 = 75, p_i = 5 atm, t_i = 40° C, 90°-Bend 66 cm From Ignitor 68

40 Rate of Flame Propagation in H_2 - O_2 Mixture; Mole % H_2 = 45, p_i = 10 atm, t_i = 40° C, 90°-Bend 66 cm From Ignitor 68

41 Rate of Flame Propagation in H_2 - O_2 Mixture; Mole % H_2 = 66.67, p_i = 10 atm, t_i = 40° C, 90°-Bend 66 cm From Ignitor 69

FIGURE Page

42 Rate of Flame Propagation in H_2 - O_2 Mixture; Mole % H_2 = 75, p_i = 10 atm, t_i = 40° C, 90°-Bend 66 cm From Ignitor 69

43 Rate of Flame Propagation in H_2 - O_2 Mixture; Mole % H_2 = 45, p_i = 1 atm, t_i = 40° C, 90°-Bend 15 cm From Ignitor 70

44 Rate of Flame Propagation in H_2 - O_2 Mixture; Mole % H_2 = 66.67, p_i = 1 atm, t_i = 40° C, 90°-Bend 15 cm From Ignitor 70

45 Rate of Flame Propagation in H_2 - O_2 Mixture; Mole % H_2 = 75, p_i = 1 atm, t_i = 40° C, 90°-Bend 15 cm From Ignitor 71

46 Rate of Flame Propagation in H_2 - O_2 Mixture; Mole % H_2 = 45, p_i = 5 atm, t_i = 40° C, 90°-Bend 15 cm From Ignitor 71

47 Rate of Flame Propagation in H_2 - O_2 Mixture; Mole % H_2 = 66.67, p_i = 5 atm, t_i = 40° C, 90°-Bend 15 cm From Ignitor 72

48 Rate of Flame Propagation in H_2 - O_2 Mixture; Mole % H_2 = 75, p_i = 5 atm, t_i = 40° C, 90°-Bend 15 cm From Ignitor 72

49 Rate of Flame Propagation in H_2 - O_2 Mixture; Mole % H_2 = 45, p_i = 10 atm, t_i = 40° C, 90°-Bend 15 cm From Ignitor 73

50 Rate of Flame Propagation in H_2 - O_2 Mixture; Mole % H_2 = 66.67, p_i = 10 atm, t_i = 40° C, 90°-Bend 15 cm From Ignitor 73

51 Rate of Flame Propagation in H_2 - O_2 Mixture; Mole % H_2 = 75, p_i = 10 atm, t_i = 40° C, 90°-Bend 15 cm From Ignitor 74

52 Coordinate System Orientation for a Flame in a Duct with an Area Discontinuity or an Obstruction 74

53 Dimensionless Induction Distance as a Function of the Correlation Function K 75

NATIONAL AERONAUTICS AND SPACE ADMINISTRATION

TECHNICAL NOTE D-1983

EXPERIMENTAL AND THEORETICAL STUDIES ON THE FORMATION OF DETONATION WAVES IN VARIABLE GEOMETRY TUBES

By

Loren E. Bollinger, Michael C. Fong,

James A. Laughrey, and Rudolph Edse

SUMMARY

16946

Detonation induction distances were obtained experimentally for hydrogen-oxygen mixtures having fuel concentrations of 45, 66.67 and 75 per cent hydrogen at initial pressures of 1 and 5 atmospheres in a detonation tube with variable internal geometry. When three stainless steel rods of different diameters were located concentrically in the initiation region of the tube, the induction distances decreased as the diameter of the rods was increased. With a divergent, stepped-wall insert placed in the initiation section of the tube, the induction distances were reduced greatly compared to those obtained in a straight cylindrical tube at 1 atmosphere initial pressure. When the tube had a right-angle section located 66 cm from the ignitor, a detonation wave formed immediately past the corner for all fuel concentrations at 1 and 5 atmospheres initial pressure except for the stoichiometric mixture at 5 atmospheres pressure for which a detonation wave formed in less than half the distance from the ignitor to the corner. A detonation wave formed again at or prior to the right-angle corner, when it was located 15 cm from the ignitor, at initial pressures of 1 and 5 atmospheres except

for 45 and 75 per cent mixtures at 1 atmosphere pressure where the induction distances were greater than those derived from the other position of the corner; however, these distances were shorter than those obtained in a cylindrical tube. Increased turbulence and the generation of stronger pressure waves from the various geometrical configurations are believed to cause the significant decrease in detonation induction distances in variable geometry tubes of the type investigated.

When a combustion wave reaches an area discontinuity or a rod-insert, pressure waves will be generated. These secondary pressure waves will lead to wave-interactions which will strongly influence the transition process from deflagration to detonation. On the basis of the small perturbation analysis, it is shown that the effects of the area disturbances generally will enhance the transition process, as verified by measurements of the detonation induction distances.

The results of the measurements of detonation induction distances with various rod-inserts and geometrical configurations are included in this analysis. It is evident that the mechanism of turbulence generation is quite important when these obstacles are placed into the flow field. Without consideration of the effects of turbulence, the transition mechanism for a flame propagating in a duct with nonuniform cross section cannot be explained satisfactorily.

EXPERIMENTAL INVESTIGATION

A. Introduction

In the study of combustion phenomena, the transition of a flame from deflagration to detonation arises as one of the more important problems. Complicating the study of this process is the fact that the transition mechanism is an unsteady process involving flame acceleration, shock-deflagration-rarefaction wave interactions, generation of turbulence and effects resulting from chemical and molecular kinetics. The distance and time required for the flame to accelerate to the detonation state is long for some mixtures and very short for others. Many factors influence the distance which is required to

establish the detonation wave from the initial deflagration flame. Some of the parameters known to have a noticeable influence on the formation of the detonation wave are the initial pressure, initial temperature, fuel concentration, type of ignition, linear flow velocity of the unburned gas in a tube, the variation in internal geometry of the tube containing the gas mixture and external magnetic fields (Refs. 1-7).

A practical parameter describing the rate of formation of a detonation wave is the detonation induction distance. As used in this report the detonation induction distance is the distance between the source of ignition and that point in the detonation tube where the propagation rate first attains a velocity which is equal to the stable detonation velocity (Chapman-Jouguet state). Interest in the formation of detonation waves arises from the technical and fundamental aspects of combustion. Results from the studies of the formation of detonation waves are expected to contribute to the understanding of combustion instability in rocket engines and to the development of engines employing detonative combustion.

The experimental portion of this investigation was conducted to determine what effect different geometric configurations of the detonation tube would have upon the detonation induction distances for various hydrogen-oxygen mixtures. With each tube configuration, numerous experiments were made at different fuel concentrations and initial pressures. Various obstacles were placed into the tube. To induce turbulence in the center of the tube and to change the cross-sectional area of the region of flow passage, three stainless steel rods were inserted concentrically in the initiation section of the detonation tube. In effect, the arrangement created an annular tube in this region. The turbulence in the expanding gas was increased by these inserts.

To study the effect of a sudden expansion of the tube cross-sectional area upon the induction distance, a divergent, stepped-wall insert was employed. With this arrangement the gas expanded suddenly when it reached the step in the insert. While the linear gas velocity decreased suddenly at these steps which reduced the formation of a detonation wave, the amount of turbulence was increased due to flow separation and eddies at the steps.

A 90-degree angle in the initiation section of the detonation tube permitted a study to be made of the effect that angular motion of the gas has upon the establishment of a stable detonation wave. In one arrangement the 90-degree corner was located only 15 cm from the ignitor while in the other set-up the corner was 66 cm distance from the source of ignition.

The results of all these experiments give an indication of the effects of these three major variations in tube configuration. Although there are many other possible geometric variations which should be investigated to permit a thorough understanding of the influence of tube geometry on the formation of detonation waves, it is believed that some of the most important ones have been selected and investigated.

B. Experimental Equipment

All of the experiments concerning the formation of detonation waves were conducted in a stainless steel tube with a 79-mm inside diameter and a wall thickness of about 2 cm; a photograph of this tube is shown in Fig. 1. For the measurements in a straight cylindrical tube, four one-meter long flanged sections were bolted together. An exploded view of one section is depicted in Fig. 2. Electric heaters, having 23 kilowatts capacity, were mounted externally on the tube sections and flanges in order to maintain the tube at a selected initial temperature. Thermocouples and an electronic temperature regulator system maintained the detonation tube at a fixed temperature of 40°C for all experiments. To maintain this temperature as accurately as possible, one-quarter-inch diameter copper tubing was wrapped around each section of the tube so that water flowing through the tubing provided an additional heat sink thereby improving the thermal lag characteristics of the control system.

The fuel and oxidizer gases were taken from standard cylinders and passed through a manifold filter to a silica gel trap to remove any oil or water vapor (Fig. 3). The silica gel trap was maintained at a low temperature by the use of a freon refrigeration system. After metering, the two gases entered the mixing vessel which was located close to the detonation tube both of which were set up in a firing pit. Appropriate valving was used so that the detonation tube could be purged with dry air, evacuated and then filled with the explosive mixture of gases. When initial pressures higher than atmospheric were needed, the tube was vented to the atmosphere through a suitably adjusted back-pressure regulator. This procedure of mixing the gases as they were needed avoided the problems and hazards of filling a high-pressure supply tank with a large amount of uniformly premixed gas for a series of experiments. Valves which were employed to seal off the detonation tube and to vent the premixed gas were operated remotely because of the danger of a possible explosion.

Probes utilizing the conduction properties of the wave were used to detect the passage of the combustion or detonation wave as illustrated in Fig. 4. A Teflon-coated wire was inserted through the wall of the tube so that the probe wire was flush with the inside surface of the tube. A 22.5-volt battery and a coaxial line to a multichannel chronograph were connected in series between the wire and ground. When the combustion or detonation wave passed the probe, the ionic content of the wave was sufficient to trigger the chronograph. The time intervals between various probe positions were determined by the difference in the chronograph readings to the respective probes. A six-channel ten-megacycle chronograph and a ten-channel one-megacycle chronograph, Fig. 5, which were developed in this laboratory, were utilized for these measurements. Details of the chronograph system can be found in Ref. 8. Probe positions were spaced along the tube at numerous places to provide adequate coverage for the velocity measurements. The type of ignitor employed for all of the experiments consisted of a 3/8-inch length of 0.005-inch diameter copper wire which was melted with current from a 28-volt D.C. power supply.

C. Tube Geometry

In the study of the effect of tube geometry on the detonation induction distances, three cylindrical rod inserts of different diameters (Figs. 6-8) and a diverging insert (Fig. 9) were located near the ignitor end of the detonation tube. The three stainless steel cylindrical bodies were mounted concentrically within the detonation tube; they extended approximately 84 cm downstream from the ignitor. The diameters of the bodies were 0.635 cm, 1.59 cm and 4.76 cm, and the ratio of the diameter of the bodies of revolution to the detonation tube diameter were 0.08, 0.20 and 0.60 respectively.

The insert containing the divergent stepped-walls (Fig. 9) was machined from aluminum stock and had an overall length of 57.42 cm. One end of the insert was located at the ignitor station. This insert provided an increase in diameter by a factor of approximately 6 in two abrupt steps. The first section of the insert, having a diameter of 1.35 cm, extended 24.13 cm downstream from the ignitor. At the end of the first section, the diameter increased to 3.81 cm which was constant for the rest of the length of the insert. The diameter then increased to 7.9 cm at the end of the insert which was the diameter of the detonation tube. Holes were drilled for the detection probe wires after the insert was assembled in the detonation tube.

An additional section which was fabricated for the detonation tube is shown in Fig. 10. It was constructed with a right-angle bend in the tube in order to study the effect of angular motion of the gas on the formation of detonation waves. The section was made from the same stainless steel stock that was used to fabricate the other four one-meter long sections of the detonation tube.

D. Experimental Procedure

In general, the same procedure was used for all experiments. After the heaters on the detonation tube were turned on, and the temperature of the tube was raised to 40°C, it was evacuated by the use of two conventional vacuum pumps. Evacuating the detonation tube shortened the flow time needed to assure a homogeneous mixture of hydrogen and oxygen in the tube, and the procedure also minimized the amount of contaminant gas. To fill the tube, the control valves on the flow stand were adjusted so that the desired flow rate for the particular fuel concentration required was obtained. Next, the premixed gas from the mixing chamber was allowed to flow into the detonation tube until the desired pressure level was obtained by employing a back-pressure regulator which allowed the gas mixture to flow out the vent when the pressure was above a predetermined level. After the explosive mixture reached the desired pressure in the tube, the gases were allowed to flow for approximately two complete changes of free volume in the tube to ensure a uniform mixture. Then, the vent and fill valves of the detonation tube were closed and the flow of gases was terminated. After the gas had reached temperature equilibrium, excess gas was bled off until the required level of initial pressure was reached. During the time needed to reach temperature equilibrium, the chronograph system was checked with the internal test system (see Ref. 1). All of the electronic equipment including the electronic gates, oscillator, pulse counters, and so forth were tested before each firing of the detonation tube. Prior to igniting the mixture, the electronic counters were reset to zero. After the explosions, the tube was vented and flushed with dry air to remove the combustion products and the next experiment was started.

During previous investigations, it was found that identical initial conditions did not give identical results in the initiation region of the detonation tube. It was established that these differences were not caused by the chronograph system. Time measurements from the region where stable detonation occurred were quite reproducible. Therefore, in order to obtain usable results it was necessary to make a number of measurements at each location of the probes for

each set of initial conditions. The velocity data from each station were averaged and graphed as a function of distance from the ignitor. In addition, the maximum and minimum values of measured velocity were indicated too. The detonation induction distance, based on the maximum propagation rates, was determined from the graphs as the point where the curve through the values of the maximum propagation rates reached the theoretical value of the detonation velocity for the particular set of initial conditions. The induction distance based on the average velocities was determined similarly. In a sense the induction distances determined from the maximum propagation rates give a "safe" induction distance if one is concerned with the destructive aspects of a detonation wave. Of course, the variation in propagation rates in the ignition region are probably not true velocity changes. The indicated variations could result from spinning flame fronts, tilted flame fronts and turbulent fronts which could have spikes of flame extending forward along the wall of the tube where the turbulence is generated by friction. The forward-protruding spikes of flame would trigger the detection probes; repeated firings with the same initial conditions would not give the same results because the formation of the flame spikes undoubtedly is a random process.

E. Results

Straight Tube Without Obstructions

Some experiments were conducted with the straight, cylindrical tube before any obstructions were placed inside. Three fuel concentrations, 45, 66.67 and 75 per cent, were employed at initial pressures of 1 and 5 atmospheres with hydrogen and oxygen. Graphs of the velocity variations are illustrated in Figs. 11 through 16. The induction distances are graphed in Figs. 27 and 28; the data are compiled in Table 1 along with the induction distances obtained from experiments with the cylindrical rod inserts.

Since the diameter affects the induction distance, a comparison can be made between the data obtained with the 79-mm tube and data obtained during previous experiments with 15-and 50-mm diameter tubes (Refs. 1 and 2) as shown in Table 2. The available induction distances are listed for both maximum and average flame propagation rates at 1 and 5 atmospheres initial pressure. No data were taken at 5 atmospheres initial pressure in the 50-mm diameter tube.

From Table 2 it can be seen that the detonation induction distances become longer as the tube diameter increases for 45 and 75 per cent fuel

concentration at both 1 and 5 atmospheres initial pressure. At stoichiometric proportions, however, the induction distances are practically the same in the 15- and 50-mm diameter tube; however, they are longer in a 79-mm diameter tube. There is no simple relationship evident from these data between detonation induction distance and tube diameter. Generally, the effect of tube diameter on detonation velocity can be expressed in terms of a linear relationship between detonation velocity and the reciprocal of the tube diameter. No such expression exists for the induction distances as the tube diameter changes.

From these limited results, it does not appear that an empirical relationship can be developed to express the dependence of detonation induction distance on tube diameter for hydrogen and oxygen mixtures. More measurements are needed to elucidate this effect.

Cylindrical Rod Inserts

A description of the three rods used is given in Section C; a cross-sectional view of their location in the tube is shown in Figs. 6 through 8. Experiments were conducted at fuel concentrations of 45, 66.67 and 75 per cent hydrogen at initial pressures of 1 and 5 atmospheres with an initial temperature of 40°C. All mixtures were ignited with the exploding wire ignitor.

Experiments with the 0.635- and 1.588-cm diameter inserts were made only with a fuel concentration of 66.67 per cent hydrogen at initial pressures of 1 and 5 atmospheres. Graphs of the average, maximum and minimum flame propagation rates as a function of distance from the ignitor are shown in Figs. 17 through 26. Also shown on these graphs are the induction distances as determined from the curves of the maximum velocities and the average velocities. These induction distances are dependent upon fuel concentration as shown in Figs. 27 and 28 respectively. The data are listed in Table 1 from which it can be seen that there is a definite decrease in the induction distances for both the 0.635- and 1.588-cm inserts compared to the induction distances without an insert at 1 atmosphere initial pressure. At 5 atmospheres, however, the induction distances for the 0.635- and 1.588-cm diameter rods decrease but not in the same proportion as those for the straight tube without obstructions which can be seen in both Figs. 27 and 28. The induction distances for these two inserts are practically equal to or greater than those for the straight tube without obstructions at 5 atmospheres even though the induction distances for the rod inserts are appreciable less than those for the same tube at 1 atmosphere pressure.

Thus, it can be seen that the effect of pressure on the induction distances is rather small when these rods were inserted in the tube as compared to the effect in a straight tube without obstructions. These results can be explained by considering the effect of turbulence which is introduced by the insertion of the rods. It is well known that increased turbulence enhances transition to detonation. It is also known that increased pressure reduces the induction distances of hydrogen-oxygen mixtures in straight tubes without obstructions. Therefore, if the transition is forced to occur in a shorter distance by turbulence (e.g., produced by cylindrical rods), then it is to be expected that the effect of pressure on the transition distance will be reduced when compared to the results obtained with straight tubes without obstructions.

During the experiments with the 0.635-cm insert, very high velocities (e.g., average velocities in excess of 10,000 meters/second) were obtained at a distance of 89.6-cm from the ignitor. These flame propagation rates were fictitious; therefore, they were not plotted on the graphs. The high apparent velocities were caused because of interference by the rod insert which was located 83.2-cm from the ignitor. If the flame front is non-planar, the detection probes on the wall of the detonation tube generate triggering signals to the chronograph which cannot be interpreted in the ordinary manner. Turbulence and shock waves from the upstream end of the rod disturbed the planar flame front. Probe signals could have been generated which gated the chronograph thereby giving rise to fictitious velocities because of the erroneous time interval.

For the 4.763-cm diameter insert, the induction distances decreased greatly compared to the results of the experiments with the 0.635- and 1.588-cm inserts. Again, similar to results obtained with the 0.635-cm insert, there were some fictitious velocities obtained at different locations downstream from the ignitor. For an initial pressure of 1 atmosphere and a fuel concentration of 66.67 per cent hydrogen, fictitious velocities were obtained at two points located 7.6 cm and 12.7 cm from the ignitor. Turbulence created by the forward end of the insert located 4 cm from the ignitor or the insert supports located at 9.08 cm from the ignitor could have caused erroneous time measurements. The same situation existed at 76.1 cm for an initial pressure of 1 atmosphere and 75 per cent fuel concentration. Also, at this initial pressure and fuel concentration, a detonation wave was formed prior to the first insert supports (9.08 cm from the ignitor) for some experiments, but not in others. Evidently the amount of turbulence created by the probe mount on the upstream end of the insert was sufficient in some cases to form a detonation wave

earlier than in other experiments. Erroneous velocities also were obtained at 7.6 cm and 12.7 cm from the ignitor for a 45 per cent fuel concentration at 5 atmospheres initial pressure and at 12.7 cm from the ignitor for a 75 per cent fuel concentration at the same initial pressure.

Divergent Insert

In order to extend the study of how internal geometry affects the induction distances in hydrogen-oxygen mixtures, an insert (Fig. 9) containing divergent stepped-walls was employed. Experiments were made at an initial pressure of 1 atmosphere only; they were discontinued after the insert was damaged when the first mixture at 5 atmospheres was detonated. The velocities obtained in the region of the insert varied considerably from experiment to experiment as shown in Figs. 29 through 31. With 45 and 66.67 per cent fuel concentrations, the velocities obtained indicated that a detonation wave was formed in the first section (1.35 cm diameter) of the insert whereas at 75 per cent fuel concentration no detonation wave was formed until the propagating flame reached the next section of the insert or was completely through the insert. Induction distances are listed in Table 3.

The effect of the insert on propagation velocity was quite evident from Figs. 29 through 31. As expected, the velocity decreased in all cases when the gas expanded at each of the two stepped-wall sections. When the gas expanded to the tube diameter, 7.9 cm, the detonation wave collapsed for the 45 and 66.67 per cent mixtures. But, the flame propagation rates indicated that the detonation started to re-form, especially with the stoichiometric mixture (Fig. 30). The detonation wave did not collapse at the end of the insert with the 75 per cent fuel mixture. Only a modest decline in velocity was obtained (Fig. 31).

Detonation induction distances determined from the maximum and average flame propagation rates in the divergent stepped-wall insert are compared with induction distances obtained in a straight tube without obstructions in Figs. 32 and 33 respectively. It is obvious from these illustrations that the induction distances with the insert are much lower than those obtained with the straight tube without obstructions. Since the 45 and 66.67 per cent mixtures detonated within the 1.35-cm diameter portion of the insert, the induction distances should be comparable to those obtained with a cylindrical tube of this same diameter without an insert. Previously, data had been obtained with hydrogen-oxygen mixtures in a 1.5-cm diameter tube. With the insert, however, the detonation induction distances are lower by factors of

from 3 to 10 than those in the 1.5-cm diameter straight tube without obstructions. The small difference in diameter from 1.5 to 1.35 cm does not appear to justify the drastic reduction in induction distance. It is believed that the large difference in induction distances results from the difference in wall roughness of the tubes. The 1.5-cm diameter tube had a very smooth wall whereas the divergent stepped-wall insert was rather rough. It was machined from aluminum, but it could not be honed. Therefore, it is believed that the resultant turbulence from the rough wall of the insert caused the detonation wave to form in a shorter distance.

Right Angle Section

To determine detonation induction distances with a right-angle section in the detonation tube, some experiments were conducted with the 90°-bend positioned 15 cm from the ignitor and additional experiments with the bend located 66 cm distant from the ignitor. Initial pressures of 1, 5 and 10 atmospheres were employed with fuel concentrations of 45, 66.67 and 75 per cent hydrogen. The initial temperature was 40°C. The propagation velocities obtained during these experiments are graphed in Figs. 34 through 51, and the induction distances are given in Table 4.

At an initial pressure of 1 atmosphere with the 90°-bend 66 cm from the ignitor, a detonation wave was formed immediately after the corner for all fuel concentrations. The induction distances for these cases were estimated to be the same for both methods of determining the induction distances (maximum and average flame propagation rates). The same results were obtained with an initial pressure of 5 atmospheres with fuel concentrations of 45 and 75 per cent. At the stoichiometric mixture, the induction distances (10 and 29 cm) were less than the distance from the ignitor to the corner. The induction distances in a straight tube for these initial conditions are 37 and 56 cm based on maximum and average propagation rates respectively (Table 1). The exact reason for this discrepancy is not known. One possible explanation is that some additional turbulence was present in this particular tube section. As anticipated from previous experiments, a detonation wave formed prior to the location of the corner for all three fuel concentrations when the initial pressure was 10 atmospheres.

With the 90°-bend located 15 cm from the ignitor, the detonation wave did not form immediately at the corner for the 45 and 75 per cent fuel concentrations at 1 atmosphere initial pressure. At the stoichiometric mixture, however, detonation occurred just downstream of the corner. Although turbulence was present at the corner, it appears that the amount was insufficient to cause transition for the lean and

fuel-rich mixtures. Ordinarily, in straight tubes without obstructions, these mixtures require a length of the order of 200 cm to detonate. At 15 cm distance, the flame propagation rates of these mixtures was not too fast and, therefore, the corner did not cause too much turbulence.

When the initial pressure was increased to 5 and 10 atmospheres, the induction distances obtained were in the general region of the right-angle corner (15 cm from the ignitor). Only at the stoichiometric mixtures did detonation occur before the corner (5 cm using the maximum propagation rates). Since no data were taken with the straight tube without obstructions at 10 atmospheres initial pressure, no comparison can be made. It is reasonable, however, to assume that the induction distance at 10 atmospheres initial pressure is near 5 cm because it is known from other experiments with hydrogen-oxygen mixtures in smaller diameter tubes that the induction distance decreases rapidly with initial pressure for stoichiometric mixtures.

F. Discussion

Cylindrical rod inserts reduce the detonation induction distance in proportion to the diameter of the insert. The primary cause of the decrease in the induction distance is the increase in the amount of turbulence which is created by the insert and its supports. With the divergent stepped-wall insert, the induction distance was reduced greatly in all experiments compared to the induction distances obtained for a straight tube without obstructions. Turbulence created by the sudden changes in area caused a reduction of the detonation induction distances.

The induction distances obtained at 1 and 5 atmospheres initial pressure with the 90°-bend at 15 cm and 66 cm from the ignitor were less than those obtained with the straight tube without obstructions. For some initial conditions, the detonation wave formed immediately past the corner while for stoichiometric mixtures it did not. At the lower pressure, apparently the turbulence was enough to lead to detonation in a shorter distance than for the straight tube. The detonation wave formed prior to the 66 cm distance at higher initial pressures which was to be expected from previous experiments. With the right-angle section 15 cm from the ignitor and the mixture at 1 atmosphere initial pressure, the distance that it took for the detonation wave to form varied considerably; these variations appear to depend on the fuel concentration and the amount of turbulence created by the corner.

Generally the overall trend with the various tube configurations employed in this investigation is a reduction in the induction distances compared to those obtained for a straight tube without obstructions.

THEORETICAL INVESTIGATION

A. Introduction

The mechanism of transition from deflagration to detonation involves the complex phenomena of wave interaction, turbulence generation, and chemical kinetics. The rationalization of any of these effects as being the predominant factor in the development of detonation waves provides a limited basis for theoretical analysis of this mechanism (Ref. 9). A comprehensive mathematical description of the inter-related phenomena leading to flame acceleration, and hence to the eventual formation of detonation waves, has not yet been explored successfully. In a different aspect, Bollinger, Fong and Edse (Ref. 6) have studied the detonation induction distances both experimentally and theoretically for various combustible mixtures in a constant-area pipe. Despite the limited scope of this approach, the transition process in terms of the induction distance can be correlated empirically to an almost universal function involving the various physical causes for flame acceleration. By "almost universal" we mean that this function exhibits an almost unique relationship with the measured induction distances, at least for the particular constant-area pipe selected for the measurements. It has been pointed out also in Ref. 6 that the empirical curve agrees fairly well with the experimental data for non-hydrocarbon systems but not for hydrocarbon systems. A tentative explanation of this peculiarity is that the possible excessive ion concentration in the unburned medium ahead of the flame front for a hydrocarbon mixture may have actuated the ionization probes prematurely, thus rendering the determination of the true induction distance much more difficult with this detection technique.

If an area change or an obstruction is present in the combustible fluid medium in which a flame propagates, additional interaction effects will arise and will be superimposed on the already existing flame acceleration process. The precompression wave will be partly transmitted and partly reflected upon reaching the area disturbance or impinging on the obstruction. The reflected wave will interact with the ensuing flame front while the transmitted wave will modify the unburned fluid medium. Thus, the flame will undergo a change in burning rate as well as in configuration, and will create compression

(or rarefaction) waves propagating both upstream and downstream of the flame front. As the flame front arrives at the cross-sectional area change or the obstruction, it will experience further changes in properties since a new set of boundary conditions for the flame front now prevails. Pressure waves emanating from the flame front will be generated whose type and strength are dictated by the particular disturbance the flame encounters.

Besides the mechanism of wave interactions, the process of turbulence generation also is expected to be intensified under these circumstances inasmuch as distortion of the flame surface, vorticity generation, flow separation, and viscous drag on the obstruction, individually or collectively, will yield a strong influence on inducing flow and flame turbulence. Without considering the effects of turbulence, erroneous conclusions may be drawn sometimes. For instance, rarefaction waves will be reflected when the precompression wave of a subsonic flame reaches an area divergence, thus causing flame deceleration. However, experimental observations have shown that the transition from deflagration to detonation is enhanced rather than delayed as predicted on the basis of the simplified inviscid wave theory.

From the foregoing physical description of the interaction phenomena with area changes (including obstructions) in an exothermic flow field, it can be foreseen that the cumulative effects will result in very complex flow patterns. On the basis of the wave-interaction analysis, the quantitative behavior of the interactions between shocks and area changes and between pressure waves and a flame discontinuity is sufficiently understood. The former has been investigated extensively by Oppenheim and Urtiew (Ref. 10), Rudinger (Ref. 11), Whitman (Ref. 12), Friedman (Ref. 13) and Rosciszewski (Ref. 14) and the latter by Rudinger (Ref. 15), and Chu (Ref. 16). In the present analysis, only the gas-dynamical aspect of the interaction between a flame and an area disturbance will be treated theoretically. A perturbation treatment following Chu's approach (Refs. 16 and 17) will be employed. While a full scope of the subject matter cannot be explored by means of the perturbation theory, it nevertheless allows an insight to be obtained of the essential features of the interaction phenomena between a flame front and area disturbances. Furthermore, the complicated calculation procedure can be circumvented with this approach.

Symbols

A	cross-sectional area of the duct
ΔA	finite change of the area
a	speed of sound
c_p	specific heat at constant pressure
D	drag force parameter due to an obstruction
d	pipe diameter
K	correlation function
L	detonation induction distance
$M_1 = \frac{W}{a_1}$	Mach number of the flame relative to unburned gas
p	pressure
Q	heat release per unit mass of medium
R	specific gas constant
$Re_1 = \frac{v_f d}{\nu}$	Reynolds number based on diameter and burning velocity
S	entropy
T	absolute temperature
T_c	flame temperature
u	gas velocity
v_f	burning velocity
$W = u_1 + v_f$	flame speed
δ	operator signifying infinitesimal change

$\epsilon = \frac{p_1}{p_2}$	pressure ratio
$\lambda = \frac{T_2}{T_1}$	temperature ratio
γ	ratio of specific heats
$\sigma = \frac{R_1}{R_2} = \frac{\mathfrak{M}_2}{\mathfrak{M}_1}$	ratio of specific gas constants across a flame front
ρ	density

Subscripts

1	conditions ahead of the flame
2	conditions behind the flame

B. Interaction Between a Subsonic Flame and a Cross-Sectional Area Change

When two ducts of different cross-sectional areas are joined together, the flow field in which a flame propagates may be described approximately by a one-dimensional model containing a discontinuous change in cross section. This simplifying assumption presupposes the existence of a plane flame front which possesses an effective flame speed determined by the chemical kinetics and transport properties of the given mixture. Upon reaching the area discontinuity, the effective flame speed is influenced further by the interaction between the flame and the partially reflected precompression wave from the area discontinuity. In this analysis, attention is directed toward the gas-dynamical aspect of flame acceleration and deflagration-to-detonation transition during the initial build-up period for a flow of combustible gases in a duct with an area change. Thus, the flame front is assumed to approach the area discontinuity with a known "effective" flame speed at a low subsonic Mach number.

Following the approach by Chu (Refs. 16 and 17), a quasi-steady, one-dimensional flow model may be selected and the coordinate system may be oriented with respect to the flame front (Fig. 52). At the instant when the flame reaches the area discontinuity, infinitesimal

changes in properties, represented by δ, are assumed to take place both upstream and downstream of the flame front. As will be seen later, many higher-order terms of the perturbation quantities, such as $\frac{\delta p_1}{p_1}$, $\frac{\delta \rho_1}{\rho_1}$, $\frac{\delta \rho_2}{\rho_2}$, ... (but not necessarily $\frac{\delta W}{W}$), can be neglected since they are small compared to unity.

The conservation of mass across a flame front located at the area transition under the steady-state condition can be expressed as

$$\rho_1 \, (u_1 + v_f) \, A = \rho_2 \, (u_2 + v_f) \, (A + \Delta A) \tag{1}$$

However, it is assumed that small changes in properties occur as soon as the flame interacts with the area disturbance. In other words, ρ_1, ρ_2, u_1, u_2 and v_f and so forth are now changed to $\rho_1 + \delta\rho_1$, $\rho_2 + \delta\rho_2$, $u_2 + \delta u_2$, and $v_f + \delta v_f$, etc. The continuity equation (1) then becomes

$$\begin{aligned} &(\rho_1 + \delta\rho_1) \, (u_1 + \delta u_1 + v_f + \delta v_f) \, A = \\ &(\rho_2 + \delta\rho_2) \, (u_2 + \delta u_2 + v_f + \delta v_f) \, (A + \Delta A) \end{aligned} \tag{2}$$

In order to reduce equation (2) to a more convenient form, the following supplementary relations are introduced:

$$u_1 + v_f = W \tag{3}$$

$$\delta u_1 + \delta v_f = \delta W \tag{4}$$

$$\delta u_2 + \delta v_f = \delta W + (\delta u_2 - \delta u_1) \tag{5}$$

$$u_2 + v_f = \frac{\rho_1}{\rho_2} \frac{A}{A + \Delta A} (u_1 + v_f) = \frac{\lambda \epsilon}{\sigma} \frac{1}{1 + \frac{\Delta A}{A}} W \tag{6}$$

$$\text{where } \epsilon = \frac{p_1}{p_2}, \ \lambda = \frac{T_2}{T_1}, \ \sigma = \frac{R_1}{R_2} \text{ and } \frac{\rho_2}{\rho_1} = \frac{\sigma}{\lambda \epsilon} \tag{7}$$

It is to be noted that the specific gas constant R as well as the specific heat c_p and the ratio of specific heats γ, which are contained in the energy and entropy equations, generally have different values in the fluid media upstream and downstream of the flame front. However, their variations are regarded as being of little practical interest.

With the aid of the relations (3) through (7) and the approximation $\left(1 + \frac{\delta\rho_2}{\rho_2}\right)^{-1} \approx 1 - \frac{\delta\rho_2}{\rho_2}$, the first-order expression for equation (2) becomes

$$\frac{\delta u_2 - \delta u_1}{W} \left(1 + \frac{\Delta A}{A}\right) = \frac{\delta W}{W} \left[\frac{\lambda \epsilon}{\sigma} - \left(1 + \frac{\Delta A}{A}\right)\right] + \left(\frac{\delta\rho_1}{\rho_1} - \frac{\delta\rho_2}{\rho_2}\right) \frac{\lambda \epsilon}{\sigma} \left(1 + \frac{\delta W}{W}\right) \tag{8}$$

For a low subsonic flame for which the dynamic contribution is neglected, the momentum equation can be obtained by integrating Euler's equation

$$A \frac{d\ (p + \delta p)}{dx} = 0 \tag{9}$$

which results in

$$\frac{\delta p_1}{p_1} = \frac{\delta p_2}{p_2} \quad \text{with } \epsilon = \frac{p_1}{p_2} = 1 \tag{10}$$

Equation (10) implies that, for a small change in cross-sectional area, the pressure pulses ahead and behind a flame front are of the same type, i.e., either both compressive or both expansive. Furthermore, this equation has the same form as that for a constant-area duct.

In a similar manner, the energy perturbation equation, ignoring the kinetic energy terms, can be expressed as follows:

$$\delta Q = c_{p_2} \delta T_2 - c_{p_1} \delta T_1 \tag{11}$$

Other conservation laws in terms of the perturbation variables are:

Entropy equation

$$\frac{\delta \rho_1}{\rho_1} = \frac{1}{\gamma_1} \frac{\delta p_1}{p_1} - \frac{\delta S_1}{c_{p_1}} \tag{12}$$

Equations of state

$$\frac{\delta \rho_1}{\rho_1} = \frac{\delta p_1}{p_1} - \frac{\delta T_1}{T_1} \tag{13}$$

$$\frac{\delta \rho_2}{\rho_2} = \frac{\delta p_2}{p_2} - \frac{\delta T_2}{T_2} \tag{14}$$

Eliminating the temperature terms from the foregoing equations, the density variation can be expressed as follows:

$$\frac{\delta\rho_1}{\rho_1} - \frac{\delta\rho_2}{\rho_2} = -\frac{\delta p_1}{p_1}\left[\frac{\gamma_1 - 1}{\gamma_1}\left(1 - \frac{c_{p_1}}{c_{p_2}}\frac{1}{\lambda}\right)\right] + \frac{\delta Q}{c_{p_2} T_1}\frac{1}{\lambda} - \frac{\delta S_1}{c_{p_1}}\left(1 - \frac{c_{p_1}}{c_{p_2}}\frac{1}{\lambda}\right) \tag{15}$$

Substitution of equation (15) into equation (8) yields

$$\frac{\delta u_2 - \delta u_1}{W}\left(1 + \frac{\Delta A}{A}\right) = \frac{\delta W}{W}\left[\frac{\lambda}{\sigma} - \left(1 + \frac{\Delta A}{A}\right)\right] - \frac{\delta p_1}{p_1}\left[\frac{\lambda}{\sigma}\frac{\gamma_1 - 1}{\gamma_1}\left(1 - \frac{c_{p_1}}{c_{p_2}}\frac{1}{\lambda}\right)\left(1 + \frac{\delta W}{W}\right)\right] - \frac{\delta S_1}{c_{p_1}}\left[\frac{\lambda}{\sigma}\left(1 - \frac{c_{p_1}}{c_{p_2}}\frac{1}{\lambda}\right)\left(1 + \frac{\delta W}{W}\right)\right] + \frac{\delta Q}{c_{p_2} T_1}\left[\frac{1}{\sigma}\left(1 + \frac{\delta W}{W}\right)\right] \tag{16}$$

It is seen that for a constant-area duct, i.e., $\Delta A = 0$, equation (16) reduces to the expression obtained by Chu (Ref. 17).

In order to analyze the type of pressure waves generated from the flame front located at the area disturbance, the perturbation quantities δW, δQ and δS_1 in equation (16) will have to be known or assumed. As a simplification, the effects of these variables on the generation of pressure waves are assumed to be additive, i.e.,

the overall effect can be treated as the sum of the individual effects. The influence of the change in flame speed on the flow characteristics under the condition of area variation will be singled out for detailed study.

It is evident that additional conditions relating the pressure waves to the velocity perturbation and the flame speed to the area change are necessary for the analysis. The former can be fulfilled by introducing the characteristic relations whereas the latter can be supplemented partially on the basis of physical considerations. Since the flame front is located at the area transition from which pressure waves are generated, the characteristic equations for plane waves can be employed to describe the pressure-velocity relationship in the two different constant-area ducts:

$$\frac{\delta p_1}{p_1} + \gamma_1 \frac{\delta u_1}{a_1} = 0 \tag{17}$$

$$\frac{\delta p_2}{p_2} - \gamma_2 \frac{\delta u_2}{a_2} = 0 \tag{18}$$

Substitution of equations (17) and (18) into equation (16) while setting $\delta Q = \delta S_1 = 0$ leads to

$$\frac{\delta p_1}{p_1} = \frac{\delta p_2}{p_2} = \left\{\gamma_1 M_1 \frac{\delta W}{W}\left[\frac{\lambda}{\sigma} - \left(1 + \frac{\Delta A}{A}\right)\right]\right\} \div \left\{\left(1 + \frac{\Delta A}{A}\right)\left(\sqrt{\frac{\gamma_1}{\gamma_2}\frac{\lambda}{\sigma}} + 1\right) + \left[\frac{\gamma_1 - 1}{\gamma_1}\left(1 - \frac{c_{p_1}}{c_{p_2}}\frac{1}{\lambda}\right)\left(1 + \frac{\delta W}{W}\right)\right]\gamma_1 M_1 \frac{\lambda}{\sigma}\right\} \tag{19}$$

where $M_1 = \frac{W}{a_1}$ is the Mach number of the flame front. It is seen that the denominator of equation (19) is always positive; therefore, whether the generated pressure waves are compressive or expansive will depend on the sign of the numerator.

According to the present coordinate orientation (Fig. 52), a sudden area convergence is represented by $\Delta A > 0$ and an area divergence is represented by $\Delta A < 0$. For low subsonic flames, δW is positive for $\Delta A > 0$ since the flow velocity increases in passing through an area constriction. Similarly, δW is negative for $\Delta A < 0$. Without any loss of generality, a simplified form of equation (19) can be obtained by assuming $\gamma = \gamma_1 = \gamma_2, \; = 1$, and ignoring the second term in the denominator because of the low Mach number and the small area variation:

$$\frac{\delta p_1}{p_1} = \frac{\delta p_2}{p_2} = \frac{\gamma M_1}{\sqrt{\lambda} + 1}\left[\frac{\lambda}{1 + \frac{\Delta A}{A}} - 1\right]\frac{\delta W}{W} \tag{20}$$

Although in the case where $\Delta A > 0$, the type of pressure waves depends on the relative magnitude between λ and $1 + \frac{\Delta A}{A}$, it appears that for most practical cases the bracketed term is positive for a small change in area. Other contributing factors which influence the determination of the type of pressure waves generated from the flame front are the changes in heat release and entropy when the area is varied. Mathematically, these effects can be analyzed by means of equation (16) and the results are similar to those for a duct having a uniform cross section (Refs. 16 and 17). In general, the following conclusions hold:

$$\left.\begin{array}{ll} \text{(i)} & \text{For area convergence, } \Delta A > 0, \; \frac{\delta p}{p} > 0 \text{ Compression} \\ \text{(ii)} & \text{For area divergence, } \Delta A < 0, \; \frac{\delta p}{p} < 0 \text{ Expansion} \end{array}\right\} \tag{21}$$

The effect of the generated pressure waves on further flame characteristics can be predicted from physical considerations. If compression waves are produced, the rearward propagating wave will be reflected from the closed end of the duct and this wave will catch up with the flame front thereby creating a new set of transmitted and reflected compression waves. Thus, the flame will be accelerated further and intermittent pressure-wave reinforcement will take place leading to the eventual formation of strong shock waves capable of auto-ignition. On the other hand, expansion waves will produce opposite effects which tend to attenuate the flame and shock intensities.

While the influence of area variation on the formation of detonation waves can be analyzed qualitatively based on the perturbation theory, this simplified fluid model selected herein may not be adequate, under certain circumstances, to explain the complex phenomena that actually exist. This aspect will be discussed further in a later section.

C. Interaction Between a Subsonic Flame and a Uniform Rod-Insert in a Constant-Area Duct

At the outset, this problem appears to be more complicated than that involving a single area discontinuity considered previously since the presence of a rod-insert not only modifies the cross-sectional area but also leads to skin friction on the surface of the rod. However, the perturbation theory still can be applied to a limited extent if the obstruction (the rod-insert) is assumed to be represented by a constant skin-friction parameter. The problem then reduces to one with an area constriction as well as that involving force and energy modifications (Fig. 52). The continuity equation remains the same as equation (2) or (8) except that the pressure ratio is of the form $\epsilon = \frac{p_1}{p_2} = \frac{p_1}{p_1 + D}$ where D is a skin-friction parameter due to the obstruction. The momentum equation based on the one-dimensional assumption then can be expressed as

$$p_1 + \delta p_1 + D = p_2 + \delta p_2 \tag{22}$$

or

$$\frac{\delta p_2}{p_2} = \epsilon \frac{\delta p_1}{p_1} \tag{23}$$

Therefore, the reflected wave represented by $\frac{\delta p_2}{p_2}$ is of the same type as the transmitted wave, $\frac{\delta p_1}{p_1}$, but the reflected wave is weaker in strength by a factor ϵ. The energy perturbation equation still can be represented by equation (11) provided that the heat addition term, Q, includes the effects due to chemical reaction as well as those resulting from viscous dissipation.

Proceding with the analysis as before, the condition which the perturbed flame must satisfy is found to be:

$$\begin{aligned}
&\frac{\delta u_2 - \delta u_1}{W}\left(1 + \frac{\Delta A}{A}\right) = \frac{\delta W}{W}\left[\frac{\lambda \epsilon}{\sigma} - \left(1 + \frac{\Delta A}{A}\right)\right] - \\
&\frac{\delta p_1}{p_1}\left\{\frac{\lambda \epsilon}{\sigma}\left[\frac{\gamma_1 - 1}{\gamma_1}\left(1 - \frac{c_{p_1}}{c_{p_2}}\frac{1}{\lambda}\right) - \left(1 - \epsilon\right)\right]\left(1 + \frac{\delta W}{W}\right)\right\} - \\
&\frac{\delta S_1}{c_{p_1}}\left[\frac{\lambda \epsilon}{\sigma}\left(1 - \frac{c_{p_1}}{c_{p_2}}\frac{1}{\lambda}\right)\left(1 + \frac{\delta W}{W}\right)\right] + \frac{\delta Q}{c_{p_2} T_1}\left[\frac{\epsilon}{\sigma}\left(1 + \frac{\delta W}{W}\right)\right]
\end{aligned} \tag{24}$$

On the basis of the argument that δW increases for an area decrease due to the presence of the rod, the simplified expression relating the generated pressure waves and the change in flame speed becomes

$$\frac{\delta p_1}{p_1} = \frac{1}{\epsilon}\frac{\delta p_2}{p_2} = \frac{\gamma M_1}{\sqrt{\lambda} + 1}\left[\frac{\lambda \epsilon}{1 + \frac{\Delta A}{A}} - 1\right]\frac{\delta W}{W} \tag{25}$$

Equation (25) shows that if ϵ is not too small and if the diameter of the rod is not too large, compression waves will be generated when the flame front reaches the rod-insert.

The limitation of the perturbation treatment must be recognized since far-reaching simplifications have been made in the analysis. The validity of a one-dimensional fluid model is questionable if the rod-insert has a relatively large diameter. Under this circumstance, the boundary-layer effect is expected to be quite pronounced and the influence of turbulence generation cannot be disregarded totally.

D. Empirical Relations

In previous studies (see Ref. 6), the transition phenomena from deflagration to detonation have been analyzed empirically. Of particular interest was the measurement of the detonation induction distance, a length parameter characterizing the development of detonation waves. It has been found that a correlation function defined as

$$K = Re_1\left(\frac{v_f}{a_1}\right)\left(\frac{T_c}{T_1}\right) \tag{26}$$

exhibits an almost unique relationship with the statistically determined detonation induction distance for a given constant-area duct. The empirical results also show that K is an almost universal function in the sense that the functional relationship holds for a number of non-hydrocarbon systems regardless of the pressure and fuel concentration. Because of insufficient data, this correlation function, K, has not been tested previously for ducts of different diameters. Recently, however, a substantial number of measurements of the detonation induction distance for various hydrogen-oxygen mixtures in constant-area ducts of diameters of 5 cm and 7.9 cm have been completed. It has been found that a dimensionless length,

$\frac{L}{d}$, where L is the induction distance, is a more suitable parameter for empirical studies. Figure 53 depicts the functional relationship between $\left(\frac{L}{d}\right)^{1/4}$ and $\left(K\right)^{1/4}$ for various hydrogen-oxygen mixtures at different pressures with d = 5 cm, 7.9 cm, and also the results obtained previously for hydrogen-oxygen and carbon monoxide - oxygen mixtures (Ref. 2) for a pipe with d = 1.5 cm. The numerical evaluations are given in Tables 3 through 6. Although the results show some scattering on the graph, the deviation of data from the average curve is not serious enough to discount the universal property of the correlation function K. One possible cause for the scattering of data comes from the calculation of K for which some of the values of the burning velocity, v_f, were extrapolated from experimental curves, and the combustion temperature, T_c, was based on theoretical calculations rather than from an experimental determination (Ref. 6). The advantage of this approach lies in the fact that the formation of detonation waves for a non-hydrocarbon mixture in a constant-area pipe can be predicted, within some degree of accuracy, by the correlation function K which depends only on the properties of the initially subsonic flame.

The empirical analysis discussed above has been extended to problems involving a non-uniform cross-sectional area and the presence of a rod-insert in a constant-area pipe. A method of superposition, similar to the determination of the wake function in turbulent flow theory, has been attempted in order to account for the influence of an area variation or an obstruction on the transition mechanism. However, in view of some of the peculiarities of the experimental results (see Table 1), a suitable correlation function has not yet been found.

E. Discussion

On the basis of the one-dimensional perturbation theory, it has been shown that the interaction between a flame front and an area change results in the generation of pressure waves propagating both upstream and downstream of the flame front. In general, compression waves are generated for area convergence and expansion waves are generated for area divergence. If the disturbance is a rod-insert, compression waves will be produced.

From equation (16) it is seen that the pressure perturbation depends on the changes in flame speed, heating value, and entropy

under the influence of an area discontinuity. As evidenced from the present mathematical procedure, the effect of an area change on wave generation cannot be predicted directly. However, it can be conceived that the non-uniformity of the geometric configuration of a duct introduces an additional condition which affects the variation of the physical quantities, such as the flame propagation rate. The latter, in turn, will determine the type of the generated pressure waves. For example, upon reaching an area convergence, the unburned gas ahead of the flame front will accelerate and the reaction zone will be thickened. Therefore, an increase in flame propagation rate will result and δW will be positive, thereby leading to the generation of compression waves as discussed previously. Mathematically speaking, the present problem can be regarded as that for a constant-area duct for which the signs of δW, δQ, and so forth, have been predetermined by the area effects. It should be mentioned that the change of flame speed through a duct with non-uniform cross section has been predicted purely on physical grounds since a rigorous mathematical analysis of this problem is not yet available.

The actual flow field for a combustion wave propagating in a duct with an area discontinuity is a very complex one. The present analysis is concerned only with the interaction between the flame and the area discontinuity under low subsonic conditions. However, as soon as combustion is initiated from the closed end, a precompression wave will be present in order to satisfy the boundary conditions. This compression wave will reach the area discontinuity before the flame front and this wave will be partially transmitted and partially reflected. With the assumption that the unburned gas flow is subsonic, the reflected wave will propagate rearward instead of being "swallowed" by the area convergence or divergence as that under high supersonic conditions.

For area convergence, the reflected wave is compressive (weak shock) which will interact with the ensuing flame front. As discussed by Rudinger (Ref. 15), the head-on collision between a shock and a flame front will distort the flame surface and the indentation will develop quickly into a spike. The flame area increases greatly and strong turbulence results. Therefore, flame acceleration occurs which will create further compression waves from the flame front. Moreover, as a result of the shock-flame interaction, rearward moving transmitted shock waves will be reflected from the closed end and will overtake the flame causing further modification of the flame front. As the flame enters into the region of a different cross-sectional area, the interplay among the area disturbance, the flame, and the shocks will result in additional waves being generated. In spite of

the complex flow field that arises, it can be foreseen that these effects will lead to the reinforcement of the intensity of the precompression wave and to a continuing acceleration of the flame. The transition from deflagration to detonation therefore is expected to be enhanced.

For area divergence, it appears that because the precompression wave is reflected from the area disturbance as rarefaction waves, the intensity of the flame may be weakened. However, for a sudden area expansion, vortices are generated and flow separation will result. Thus, the mechanism of turbulence generation will compensate for the weakening of the shock (precompression wave) intensity due to the wave-interaction phenomena. The final outcome still is the enhancement of the transition process from deflagration to detonation. Indeed, the experimental measurement of the detonation induction distance for hydrogen-oxygen combustion waves through a duct with sudden area enlargement clearly confirms this conclusion.

If a uniform rod is inserted symmetrically in a constant-area duct, the effects are manifold:

(1) The cross-sectional area is reduced as if two uniform ducts of different cross-sectional area were joined together,

(2) The precompression wave as well as the flame will impinge on the obstruction (the front surface of the rod-insert) causing a series of wave-interaction phenomena,

(3) The rod-insert furnishes an additional source of real gas effects, such as the effects from viscous stresses and heat transfer.

From a qualitative viewpoint, the transition phenomena can be analyzed or at least predicted by considering the individual effects listed above. The wave-interaction aspect of the problem follows the same procedure as before, but the generation of turbulence is determined partially by the shape and the diameter of the rod-insert. For larger diameter rod-inserts, the heat-sink effect becomes more significant, and the one-dimensional flow model may be inadequate to describe the flow field fully.

Whether the disturbance is caused by area discontinuity or by a rod-insert, it can be concluded that the transition from deflagration to detonation generally will be enhanced as compared with that for a constant-area duct. Without sufficient quantitative information about the effects of area change and obstruction on flow disturbances, the

problem is not amenable to empirical analysis at the present time. Also some difficulties were encountered in the determination of the detonation induction distances for a larger diameter rod-insert ($d = 4.76$ cm) for which two sets of additional supports had to be used in order to center the rod. The measured velocities near these supports were found to have large values locally which indicate a different experimental condition from that without these supports. The task of determining the induction distance accurately, therefore, was quite difficult.

Although some understanding can be gained by employing the method of characteristics to analyze the interaction phenomena between a flame front and an area disturbance or obstruction, the calculated flow patterns still are very likely to deviate from the real ones. In particular, the important role of the turbulence generation under these circumstances cannot be incorporated easily to the graphical and iteration procedures.

CONCLUSIONS

When a combustion wave reaches an area discontinuity or a rod-insert, pressure waves will be generated. These generated pressure waves will induce subsequent wave-interaction phenomena which will strongly influence the transition process from deflagration to detonation. On the basis of the small perturbation analysis, it is shown that the effects of the area disturbances generally will enhance the transition process, as verified by measurements of the detonation induction distances.

The results of the measurements of detonation induction distances with various rod-inserts and geometrical configurations are included in this analysis. It is evident that the mechanism of turbulence generation is quite important when these disturbances are present in the flow field. Without consideration of the effects of turbulence, the transition mechanism for a flame propagating in a duct with non-uniform cross section cannot be explained satisfactorily.

The simplified flow model selected for theoretical analysis of the interaction phenomena between a low subsonic combustion wave and area disturbances permits a qualitative understanding of the complicated problem. Although a general trend of the transition process from deflagration to detonation due to area effects (including an obstruction) can be predicted according to the perturbation theory, a great

improvement in the analysis can be achieved if viscous effects are incorporated therein.

Some of the data from the measurements of the detonation induction distances (Table 1) show surprising results. For example, the induction distance for a stoichiometric hydrogen-oxygen mixture at 5 atmospheres initial pressure varies in a somewhat inconsistent manner with the change in the diameter of the rod-insert. At 5 atmospheres pressure, the induction distances increase with the amount of blockage until the rod-insert with 60 per cent blockage is employed whereupon the induction distance decreases drastically. Because of the limited amount of data available and until a satisfactory explanation of this peculiarity is given, it is difficult to develop an empirical formula similar to that for a constant-area duct.

The Ohio State University
Rocket Research Laboratory
Columbus 10, Ohio August 1, 1962

REFERENCES

1. Bollinger, L. E., and Edse, R.: Measurement of Detonation Induction Distances in Hydrogen-Oxygen and Acetylene-Oxygen-Nitrogen Mixtures At Normal and Elevated Initial Pressures and Temperatures, Wright Air Development Center Technical Report 57-414, ASTIA No. AD 130874, June 1957.

2. Bollinger, L. E., and Edse, R.: Detonation Induction Distances in Combustible Gaseous Mixtures at Atmospheric and Elevated Initial Pressures. I Methane-Oxygen, II Carbon Monoxide - Oxygen, III Hydrogen-Oxygen, Wright Air Development Center Technical Report 58-591, ASTIA No. 208325, March 1959.

3. Bollinger, L. E., Fong, M. C., and Edse, R.: Detonation Induction Distances in Combustible Gaseous Mixtures at Atmospheric and Elevated Initial Pressures. IV Hydrogen - Nitric Oxide, V Hydrogen-Oxygen-Diluent, VI Theoretical Analysis. Wright Air Development Center Technical Report 58-591 (Part II), ASTIA No. AD 239677, Aug. 1959.

4. Bollinger, L. E., Fong, M. C., and Edse, R.: Theoretical Analysis and Experimental Measurements of Detonation Induction Distances at Atmospheric and Elevated Initial Pressures, American Rocket Society Meeting, Washington, D. C., 16-20 Nov. 1959, Paper No. 922-59.

5. Bollinger, L. E., and Edse, R.: Thermodynamic Calculations of Hydrogen-Oxygen Detonation Parameters for Various Initial Pressures, ARS Journal, 31, No. 2, pp. 251-256, Feb. 1961.

6. Bollinger, L. E., Fong, M. C., and Edse, R.: Experimental Measurements and Theoretical Analysis of Detonation Induction Distances, ARS Journal, 31, No. 5, pp. 588-595, May 1961.

7. Fong, M. C., Bollinger, L. E., and Edse, R.: Magnetohydrodynamic Effects on Exothermal Waves. I Theoretical Problems on a Macroscopic Scale, II Experimental Study with Hydrogen-Oxygen Detonation Waves. Aeronautical Research Laboratory Technical Report 69, ASTIA No. AD 269280, Sept. 1961.

8. Bollinger, L. E.: A Six Channel, Ten-Megacycle Chronograph for Supersonic Velocity Measurements. Eleventh Annual I.S.A. Conference, New York City, 17-21 Sept. 1956.

9. Oppenheim, A. K., and Stern, R. A., On the Development of Gaseous Detonation--Analysis of Wave Phenomena. Seventh Symposium (International) on Combustion. Butterworths Scientific Publications, London, 1959, pp. 837-850.

10. Oppenheim, A. K., and Urtiew, P. A., Vector Polar Method for Shock Interactions with Area Disturbances. AFOSR TN 59-701, Technical Note DR 4, University of California, Berkeley, July 1959.

11. Rudinger, G., Wave Diagrams for Nonsteady Flows in Ducts, D. Van Nostrand Co., Inc., New York, 1955.

12. Whitman, G. B., On the Propagation of Shock Waves through Regions of Non-uniform Area of Flow, Journal of Fluid Mechanics, Vol. 4, Part 4, Aug. 1958, pp. 337-360.

13. Friedman, M. P., An Improved Perturbation Theory for Shock Waves Propagating Through Non-uniform Regions. Journal of Fluid Mechanics, Vol. 8, Part 2, 1960, pp. 193-209.

14. Rościszewski, J., Calculations of the Motion of Non-uniform Shock Waves, Journal of Fluid Mechanics, Vol. 8, Part 3, 1960, pp. 337-367.

15. Rudinger, G., Shock Wave and Flame Interactions, Combustion and Propulsion, Third AGARD Colloquium, Pergamon Press, 1958.

16. Chu, B. T., On the Generation of Pressure Waves at a Plane Flame Front, Fourth Symposium (International) on Combustion, Williams and Wilkins Co., Baltimore, 1953, pp. 603-612.

17. Chu, B. T., Mechanism of Generation of Pressure Waves at Flame Fronts, NACA TN 3683, Oct. 1960.

TABLE 1. DETONATION INDUCTION DISTANCES FOR CYLINDRICAL ROD INSERTS

Initial Conditions			Detonation Tube Configuration							
t_i °C	p_i atm	Mixture Mol Per Cent Hydrogen	Without Insert Induction Distance (cm)		d/D = 0.08 Induction Distance (cm)		d/D = 0.20 Induction Distance (cm)		d/D = 0.60 Induction Distance (cm)	
			(a)	(b)	(a)	(b)	(a)	(b)	(a)	(b)
40	1	45	186	211	ND	ND	ND	ND	32	33
		66.67	137	166	94	96	60	68	16	17
		75	207	213	ND	ND	ND	ND	7	78
40	5	45	86	92	ND	ND	ND	ND	16	16
		66.67	37	56	47	64	51	53	7	30
		75	90	94	ND	ND	ND	ND	6	7

a Induction distances determined from maximum flame propagation rates

b Induction distances determined from average flame propagation rates

d diameter of body

D diameter of detonation tube = 79 mm

ND No data taken

TABLE 2. COMPARISON OF DETONATION INDUCTION DISTANCES FOR HYDROGEN-OXYGEN MIXTURES IN CYLINDRICAL TUBES OF DIFFERENT DIAMETER

Initial Conditions			Induction Distances (cm)					
t_i °C	p_i atm	Mixture Mol Per Cent Hydrogen	Based on Maximum Flame Propagation Rates			Based on Average Flame Propagation Rates		
			Detonation Tube Diameter			Detonation Tube Diameter		
			15 mm	50 mm	79 mm	15 mm	50 mm	79 mm
40	1	45	82	106	186	15	108	211
		66.67	74	72	137	104	93	166
		75	95	165	207	125	170	213
40	5	45	29	ND	86	32	ND	92
		66.67	19	ND	37	20	ND	56
		75	35	ND	90	33	ND	94

ND No data taken

TABLE 3. DETONATION INDUCTION DISTANCES FOR THE DIVERGING INSERT

Initial Conditions			Detonation Tube Configuration			
t_i °C	p_i atm	Mixture Mol Per Cent Hydrogen	Without Insert Induction Distance (cm)		With Insert Induction Distance (cm)	
			(a)	(b)	(a)	(b)
40	1	45	186	211	8	11
		66.67	137	166	13	23
		75	207	213	25	36

(a) Induction distances determined from maximum flame propagation rates

(b) Induction distances determined from average flame propagation rates

TABLE 4. DETONATION INDUCTION DISTANCES FOR THE RIGHT ANGLE SECTION CONFIGURATION

Initial Conditions			Location of Right Angle from the Ignitor (cm)			
			15		66	
t_i °C	p_i atm	Mixture Mol Per Cent Hydrogen	Induction Distance (cm)		Induction Distance (cm)	
			(a)	(b)	(a)	(b)
40	1	45	32	118	70	70
		66.67	20	20	70	70
		75	20	199	70	70
	5	45	12	17	70	70
		66.67	18	18	10	29
		75	13	17	70	70
	10	45	14	17	39	50
		66.67	5	15	10	14
		75	16	18	39	44

(a) Induction distances determined from maximum flame propagation rates

(b) Induction distances determined from average flame propagation rates

TABLE 5. EVALUATION OF $\left(K\right)^{\frac{1}{4}}$ AND $\left(\frac{L}{d}\right)^{\frac{1}{4}}$ FOR VARIOUS HYDROGEN-OXYGEN MIXTURES (d = 1.5 cm)

Mol Per Cent Hydrogen	p_1 (atm)	L (cm)	K	$\left(\frac{L}{d}\right)$	$\left(\frac{L}{d}\right)^{\frac{1}{4}}$	$\left(K\right)^{\frac{1}{4}}$
40.0	1	102	276.9	68	2.87	4.07
	5	41	3076.0	27.3	2.28	7.42
	10	36	9409.5	24	2.22	9.85
	25	-	44315.1	-	-	14.5
50.0	1	66	481.0	44	2.58	4.68
	5	20	5508.4	13.3	1.91	8.61
	10	13.5	16714.6	9	1.73	11.37
	25	5	79839.1	3.4	1.36	16.79
60.0	1	61	1026.8	40.6	2.52	5.66
	5	16	9340.2	10.67	1.81	9.82
	10	13	25663.6	8.68	1.72	12.65
	25	5	108187.6	3.4	1.36	18.13
66.7	1	-	1278.2	-	-	5.97
	5	19	9565.8	12.66	1.89	9.88
	10	12	24767.0	8.0	1.68	12.54
	25	2.5	95239.3	1.67	1.14	17.58
70.0	1	91	1222.4	60.7	2.79	5.91
	5	20	7510.4	13.3	1.91	9.3
	10	13	18317.5	8.68	1.72	11.64
	25	4	69281.4	2.67	1.28	16.23
80.0	1	156	290.6	104	3.19	4.18
	5	53	1743.8	35.35	2.44	6.45
	10	45	3869.5	30	2.34	7.9
	25	31	12113.0	20.65	2.13	10.52

Values of L and K are obtained from Ref. 6.

TABLE 6. EVALUATION OF $\left(K\right)^{\frac{1}{4}}$ AND $\left(\frac{L}{d}\right)^{\frac{1}{4}}$ FOR VARIOUS HYDROGEN-OXYGEN MIXTURES (d = 5.0 cm)

Mol Per Cent Hydrogen	p_1 (atm)	L (cm)	K	$\left(\frac{L}{d}\right)$	$\left(\frac{L}{d}\right)^{\frac{1}{4}}$	$\left(K\right)^{\frac{1}{4}}$
45.0	1	100	1315	20	2.11	6.02
60.0	1	50	3420	10	1.78	7.65
66.7	1	70	4260	14	1.93	8.07
70.0	1	70	4080	14	1.93	7.96
75.0	1	166	2135	33.2	2.4	6.80
80.0	1	290	987	58	2.76	5.60

Values of L are obtained from Ref. 2.

TABLE 7. EVALUATION OF $\left(K\right)^{\frac{1}{4}}$ AND $\left(\frac{L}{d}\right)^{\frac{1}{4}}$ FOR

VARIOUS HYDROGEN-OXYGEN MIXTURES (d = 7.9 cm)

Mol Per Cent Hydrogen	p_1 (atm)	L (cm)	K	$\left(\frac{L}{d}\right)$	$\left(\frac{L}{d}\right)^{\frac{1}{4}}$	$\left(K\right)^{\frac{1}{4}}$
45.0	1	186	1922	23.55	2.2	6.62
	5	86	21900	10.9	1.82	12.16
66.7	1	137	6720	17.33	2.04	9.05
	5	37	50300	4.7	1.47	14.97
75.0	1	207	3365	26.2	2.26	7.61
	5	90	24200	11.4	1.84	12.48

TABLE 8. EVALUATION OF $\left(K\right)^{\frac{1}{4}}$ AND $\left(\frac{L}{d}\right)^{\frac{1}{4}}$ FOR

VARIOUS CARBON MONOXIDE - OXYGEN MIXTURES (d = 1.5 cm)

Mol Per Cent Carbon Monoxide	p_1 (atm)	L (cm)	K	$\left(\frac{L}{d}\right)$	$\left(\frac{L}{d}\right)^{\frac{1}{4}}$	$\left(K\right)^{\frac{1}{4}}$
45.0	5	156	57.8	104	3.20	2.76
	10	141	128.7	94.0	3.12	3.37
	25	107	388.6	71.3	2.91	4.44
60.0	5	129	123.2	86.0	3.04	3.33
	10	122	318.2	81.3	3.00	4.26
	25	74	1294.5	49.3	2.65	6.00
66.7	5	125	152.7	83.3	3.02	3.51
	10	117	392.4	79.0	2.98	4.46
	25	61	1703.1	40.7	2.52	6.42
75.0	5	143	172.3	95.3	3.12	3.62
	10	125	441.8	83.3	2.65	4.58
	25	114	1917.8	76.0	2.95	6.61
80.0	5	154	147.3	102.7	3.18	3.48
	10	145	356.3	96.7	3.14	4.35
	25	126	1349.7	84.0	3.02	6.05

Values of L and K are obtained from Ref. 6.

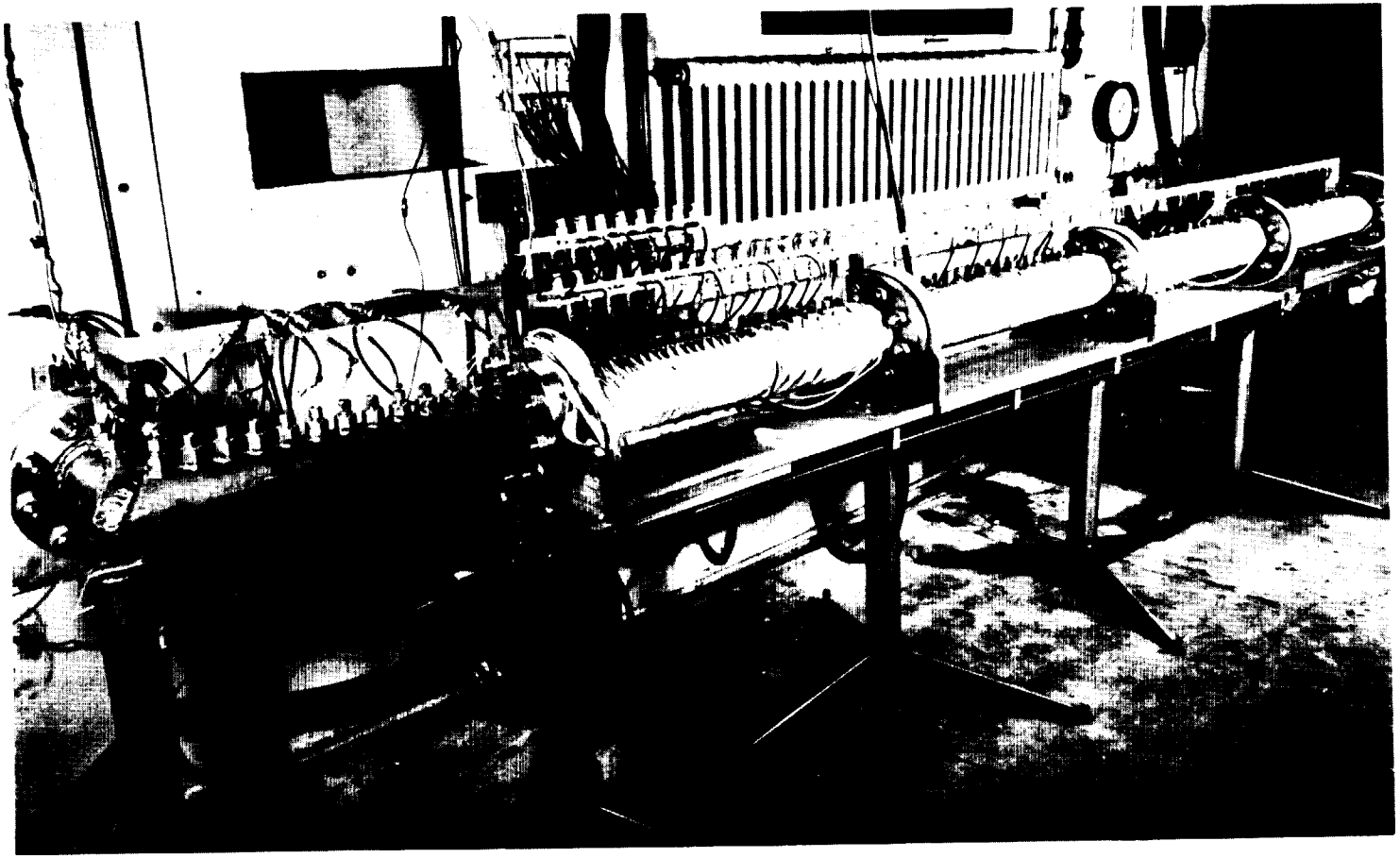

FIG. 1 PHOTOGRAPH OF DETONATION TUBE

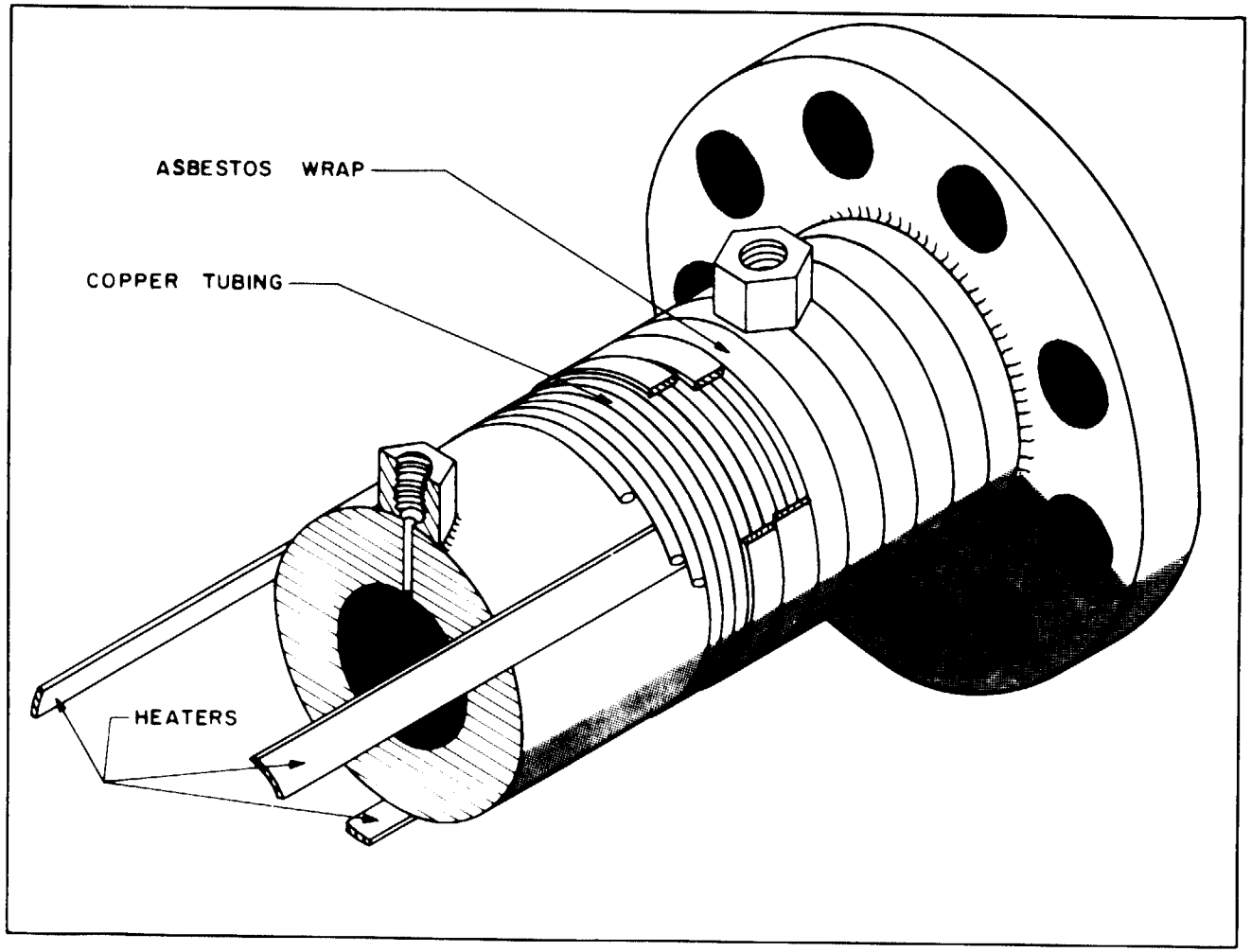
ASBESTOS WRAP
COPPER TUBING
HEATERS

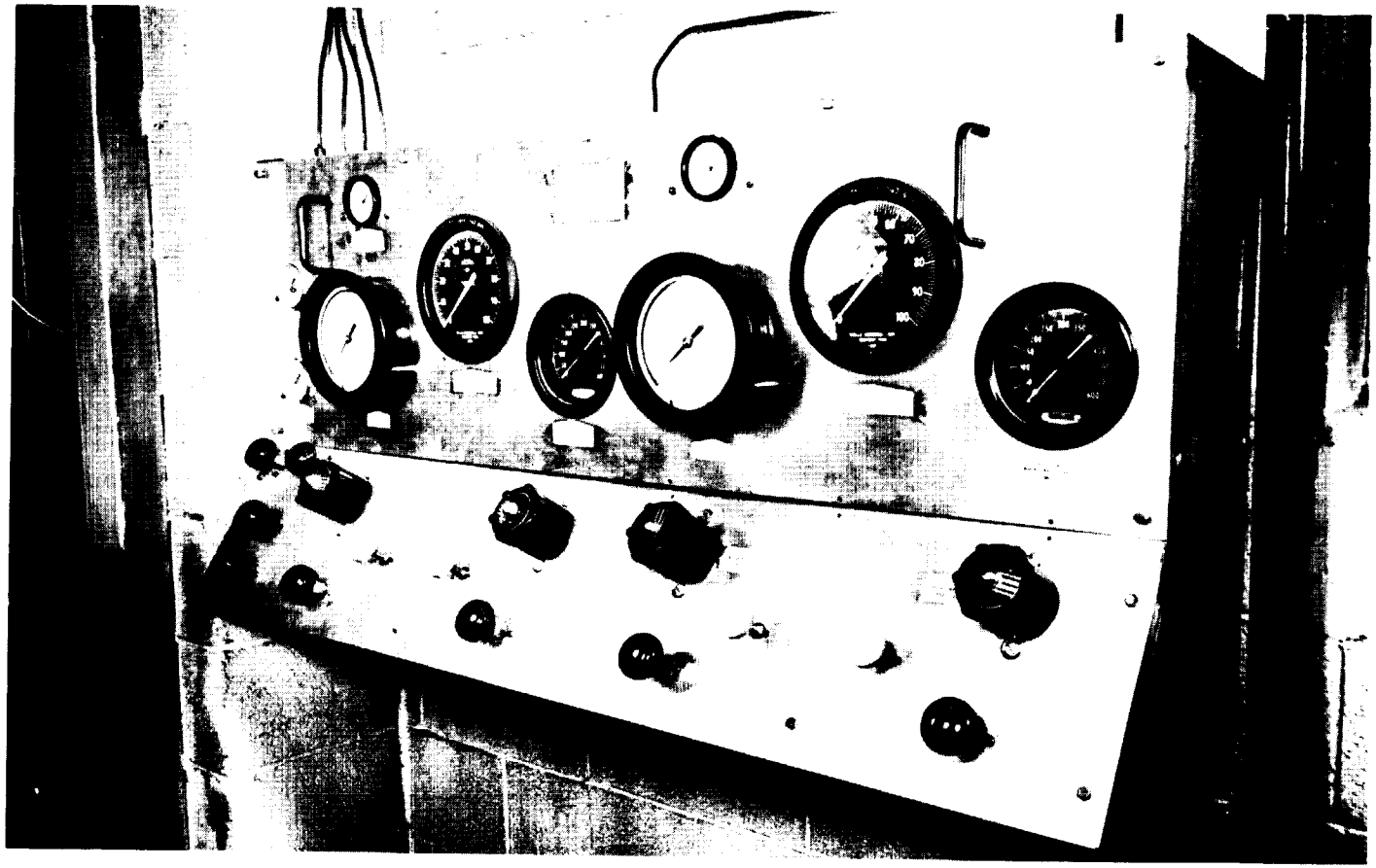

FIG. 3 PHOTOGRAPH OF FLOW CONTROL SYSTEM

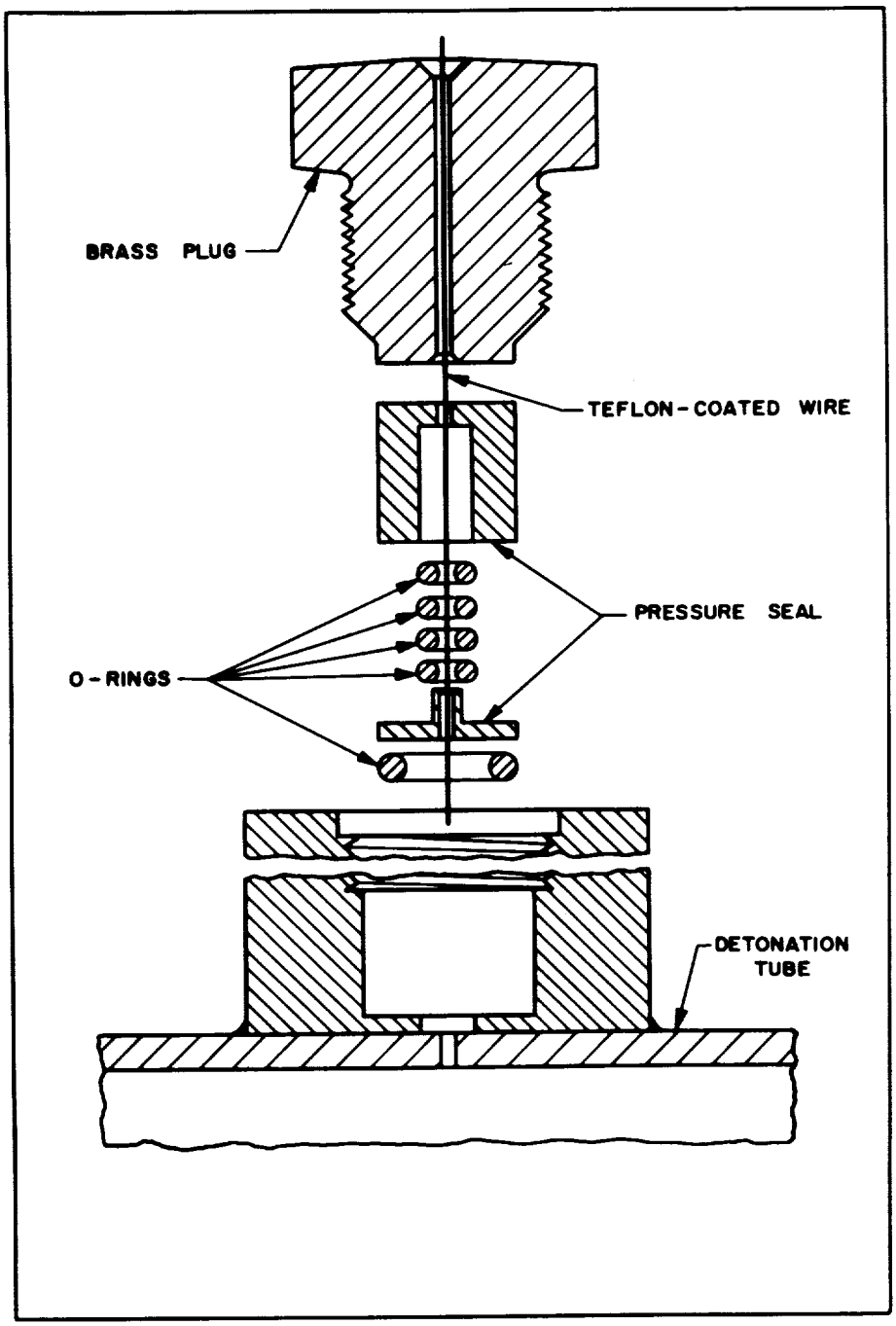

FIG. 4 EXPLODED VIEW OF PROBE ASSEMBLY

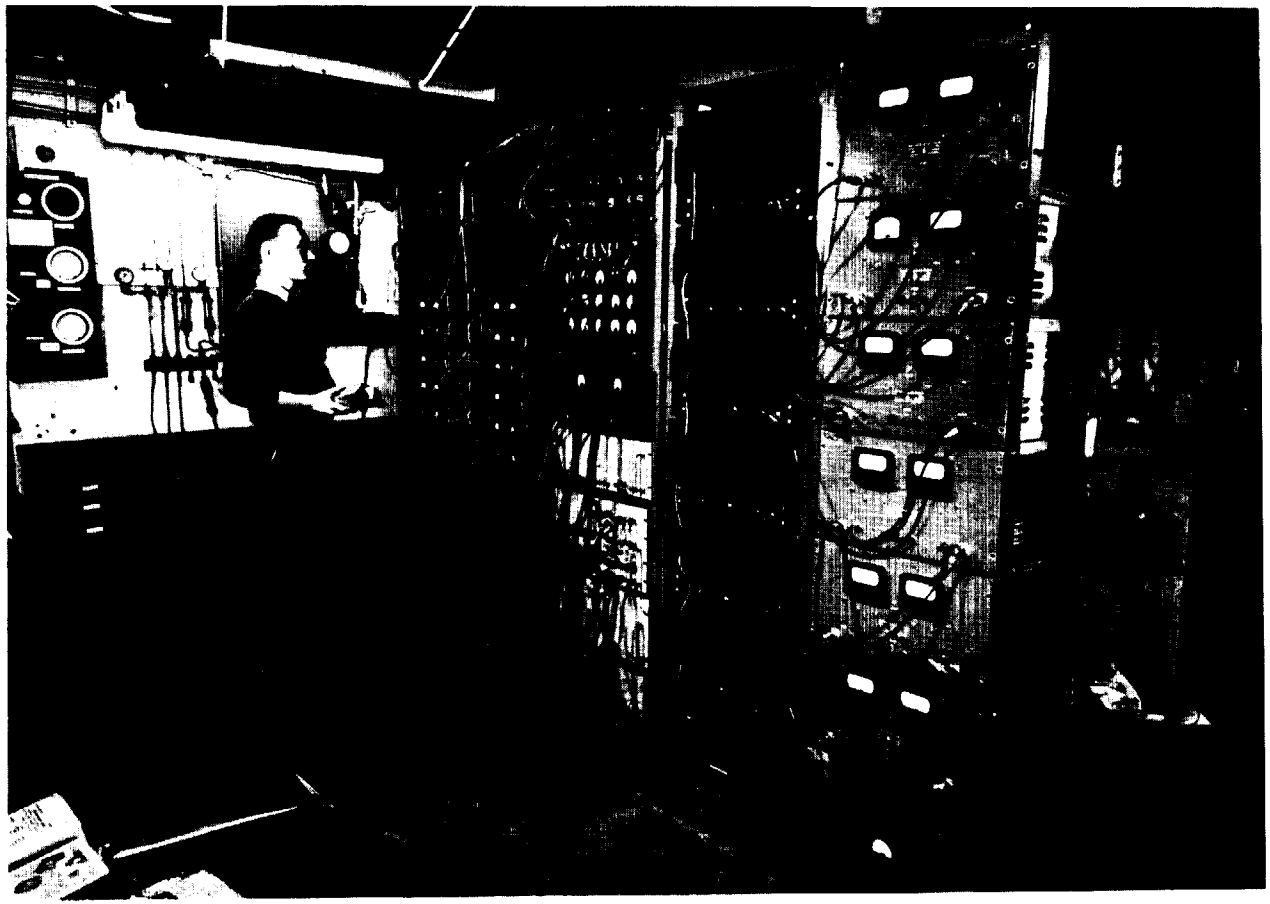

FIG. 5 PHOTOGRAPH OF CHRONOGRAPH SYSTEM

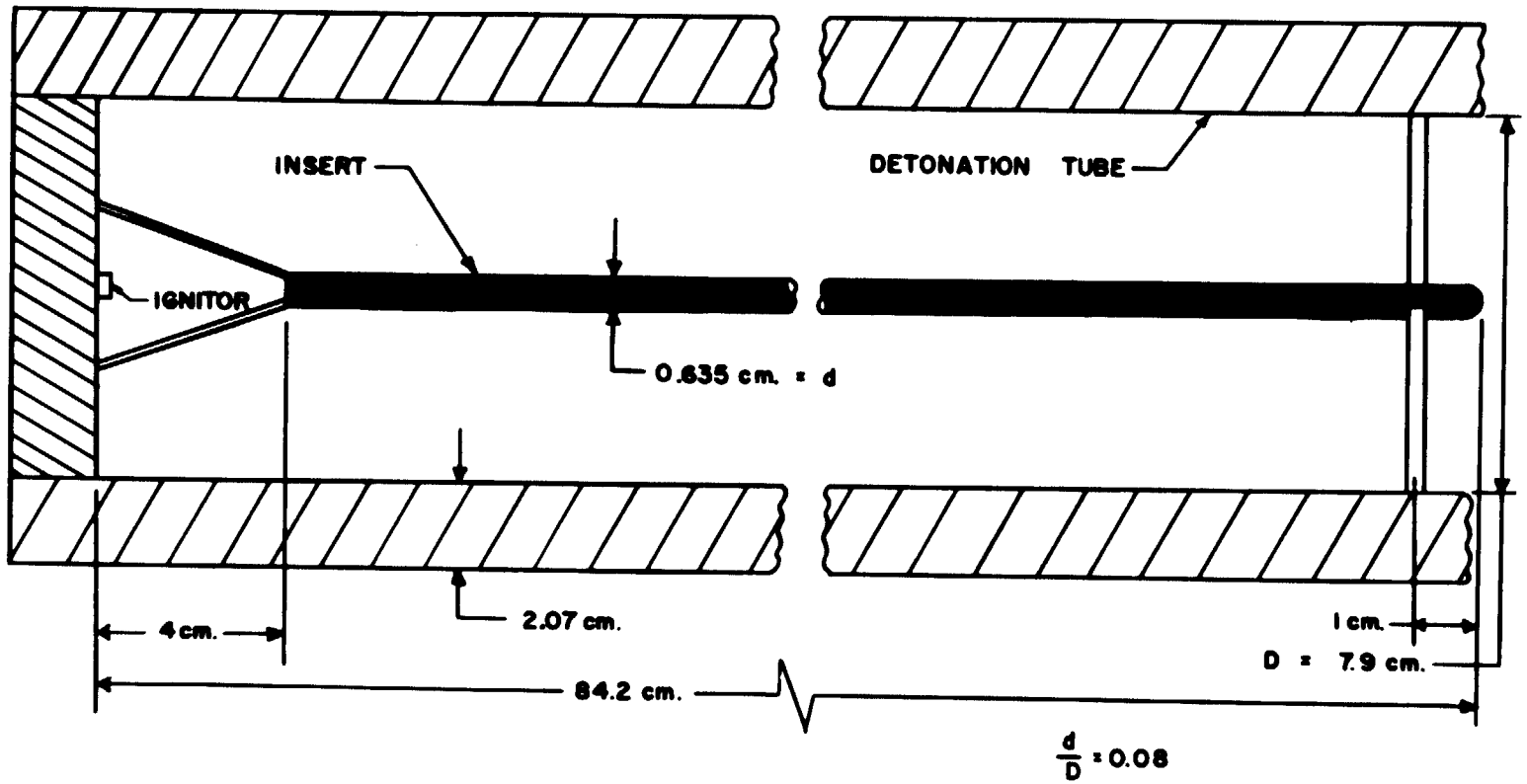

FIG. 6 DESCRIPTIVE VIEW OF CYLINDRICAL INSERT, DIAMETER = 0.635 CM

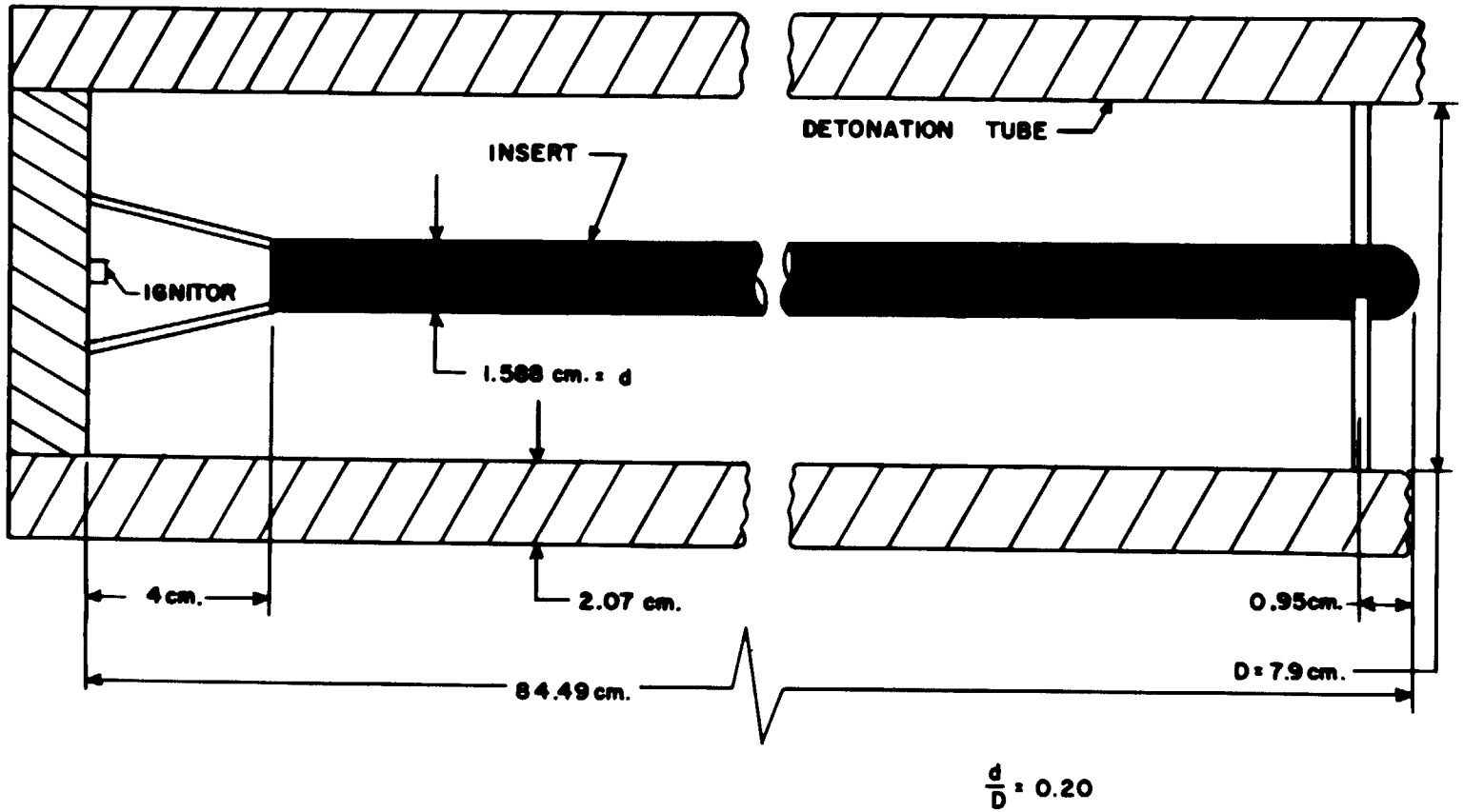

FIG. 7 DESCRIPTIVE VIEW OF CYLINDRICAL INSERT, DIAMETER = 1.588 CM

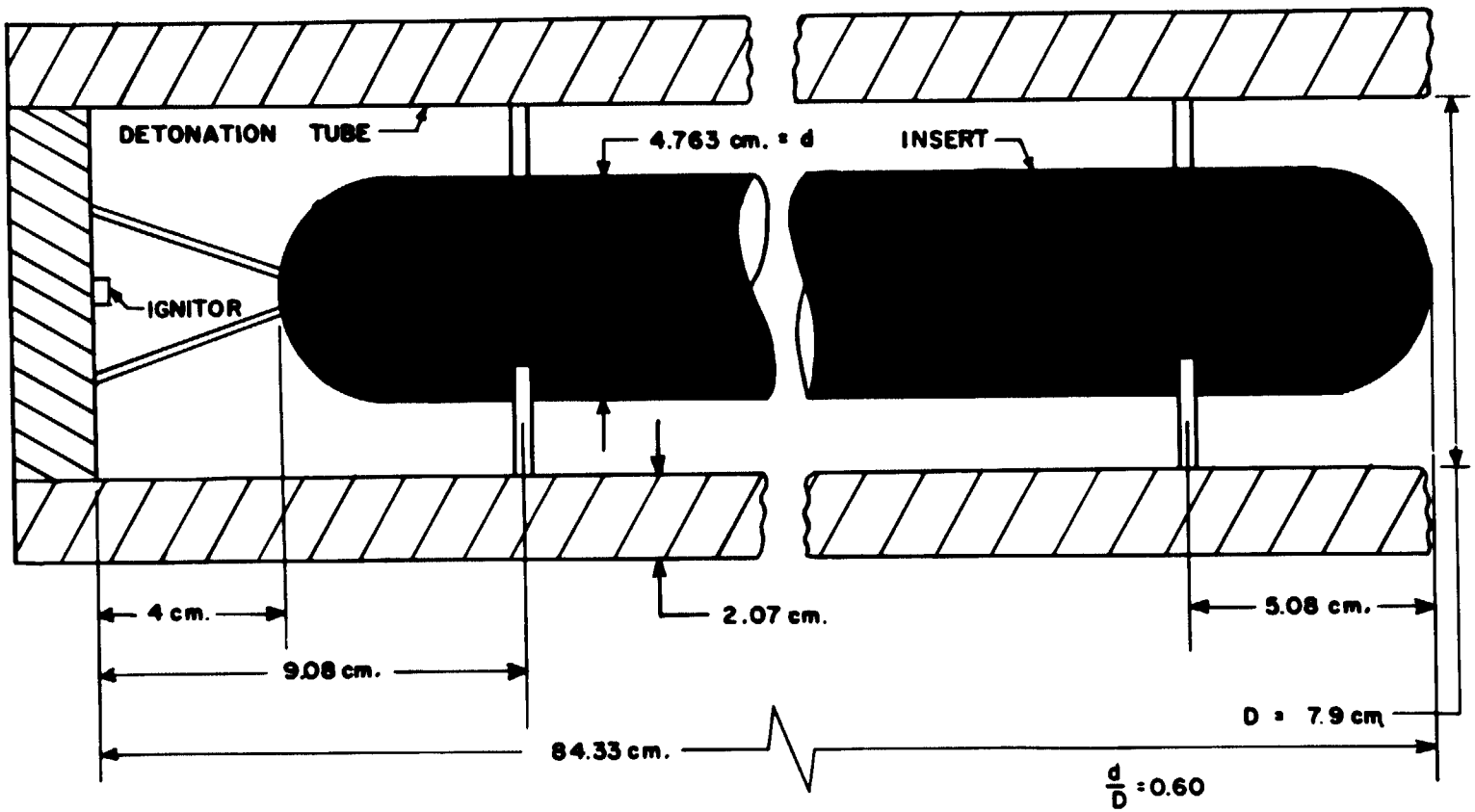

FIG. 8 DESCRIPTIVE VIEW OF CYLINDRICAL INSERT, DIAMETER = 4.763 CM

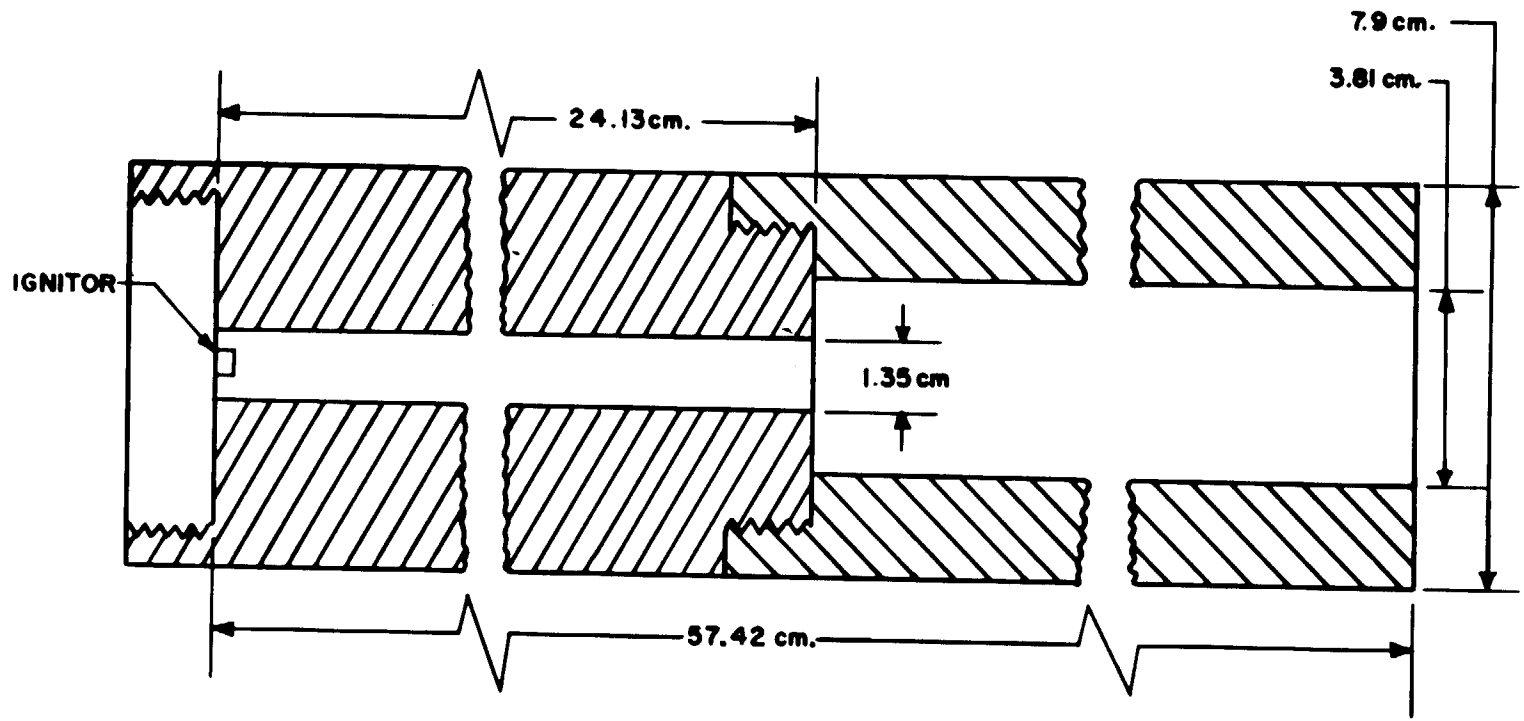

FIG. 9 DESCRIPTIVE VIEW OF DIVERGENT STEPPED-WALL INSERT

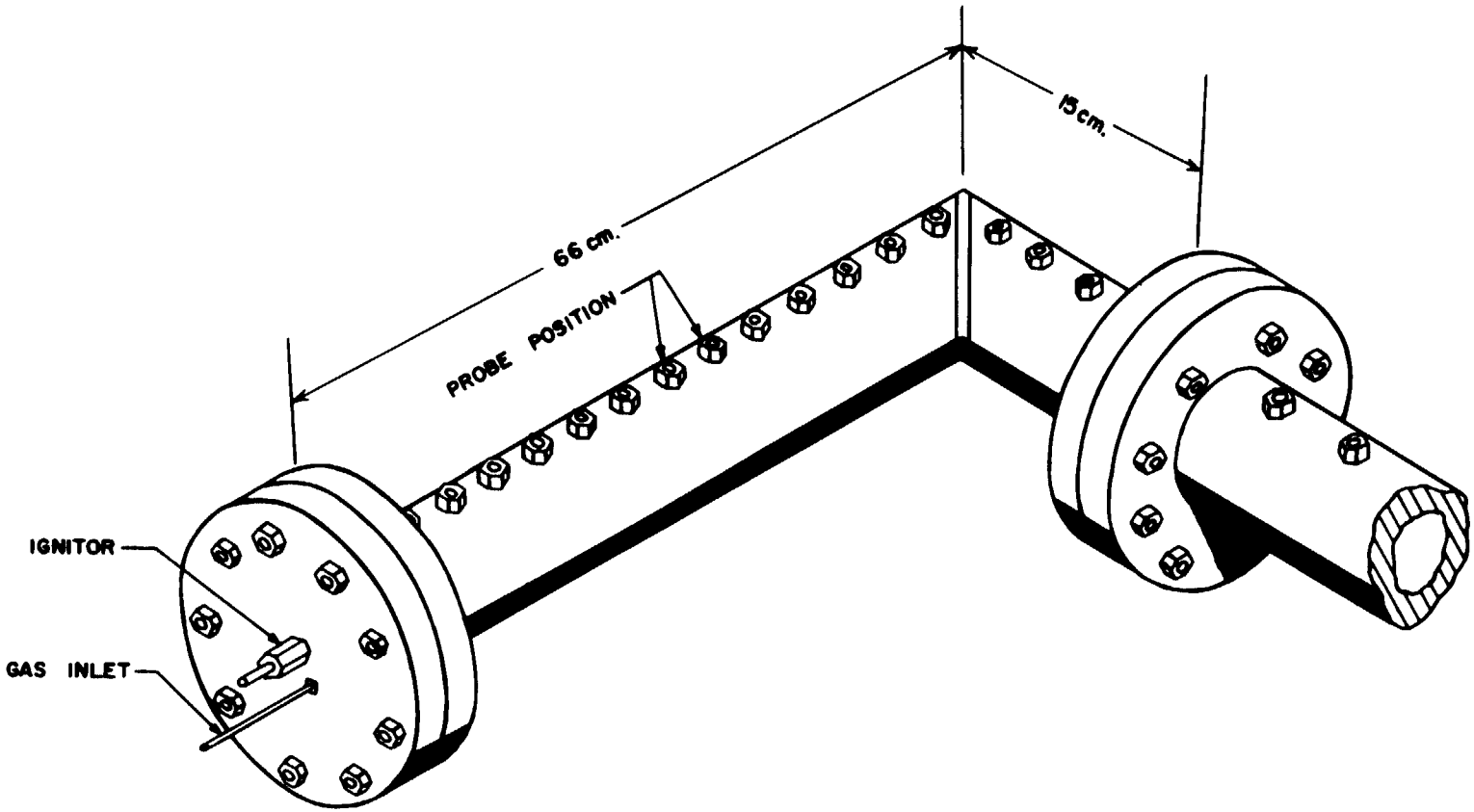

FIG. 10 RIGHT-ANGLE SECTION FOR DETONATION TUBE

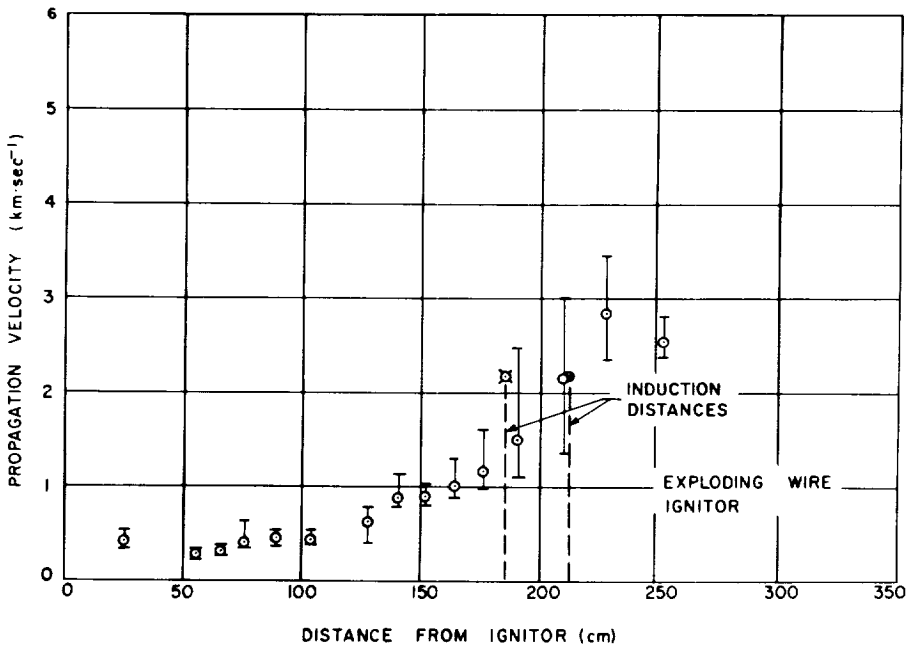

FIG. 11 RATE OF FLAME PROPAGATION IN H_2 - O_2 MIXTURE; MOLE % H_2 = 45, p_i = 1 ATM, t_i = 40°C, CLEAR TUBE.

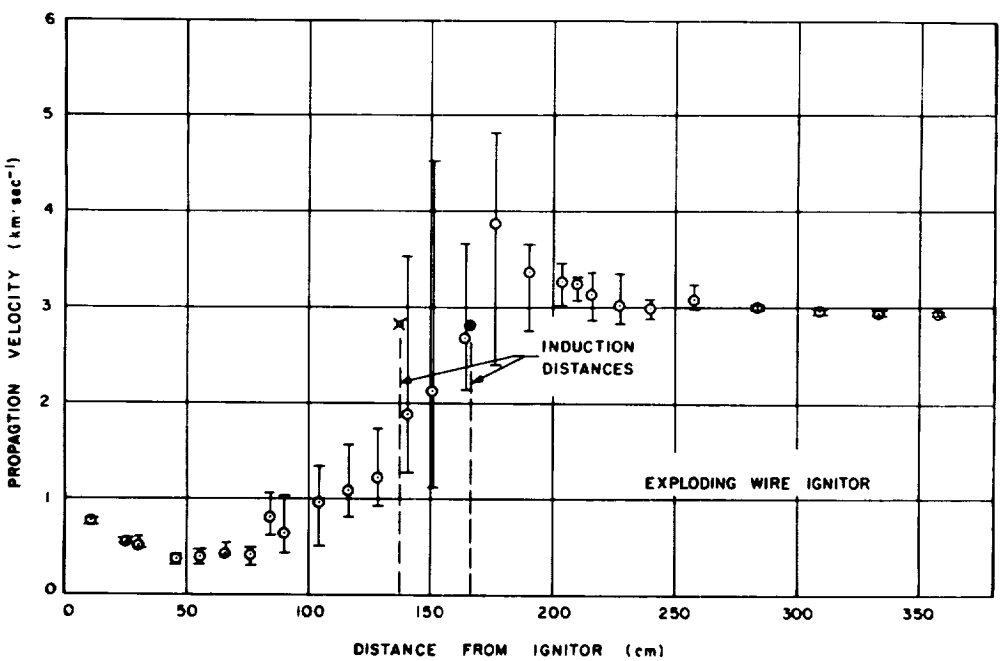

FIG. 12 RATE OF FLAME PROPAGATION IN H_2 - O_2 MIXTURE; MOLE % H_2 = 66.67, p_i = 1 ATM, t_i = 40°C, CLEAR TUBE.

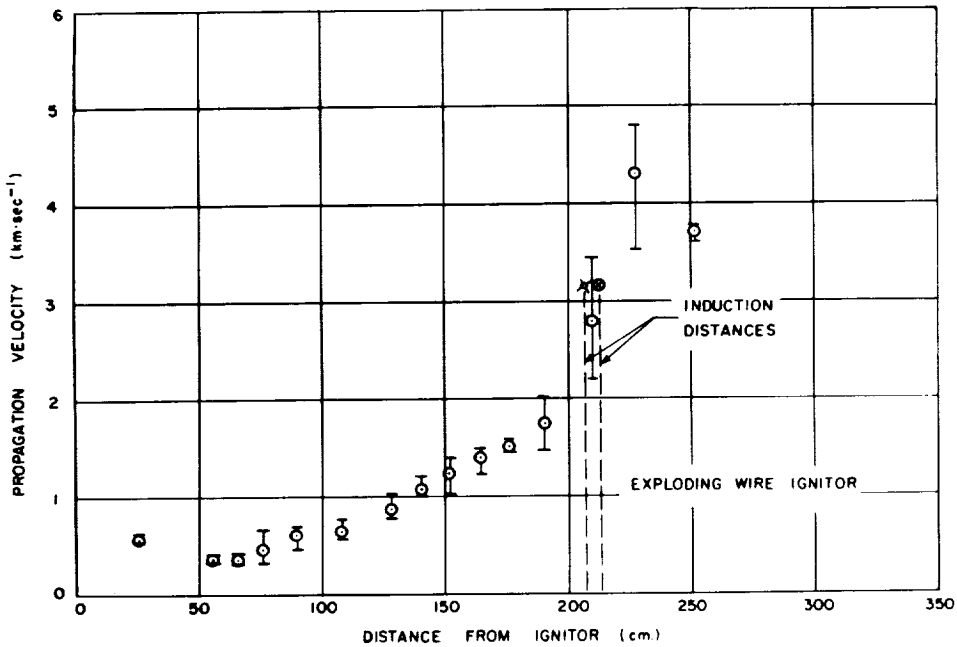

FIG. 13 RATE OF FLAME PROPAGATION IN H_2 - O_2 MIXTURE; MOLE % H_2 = 75, p_i = 1 ATM, t_i = 40°C, CLEAR TUBE.

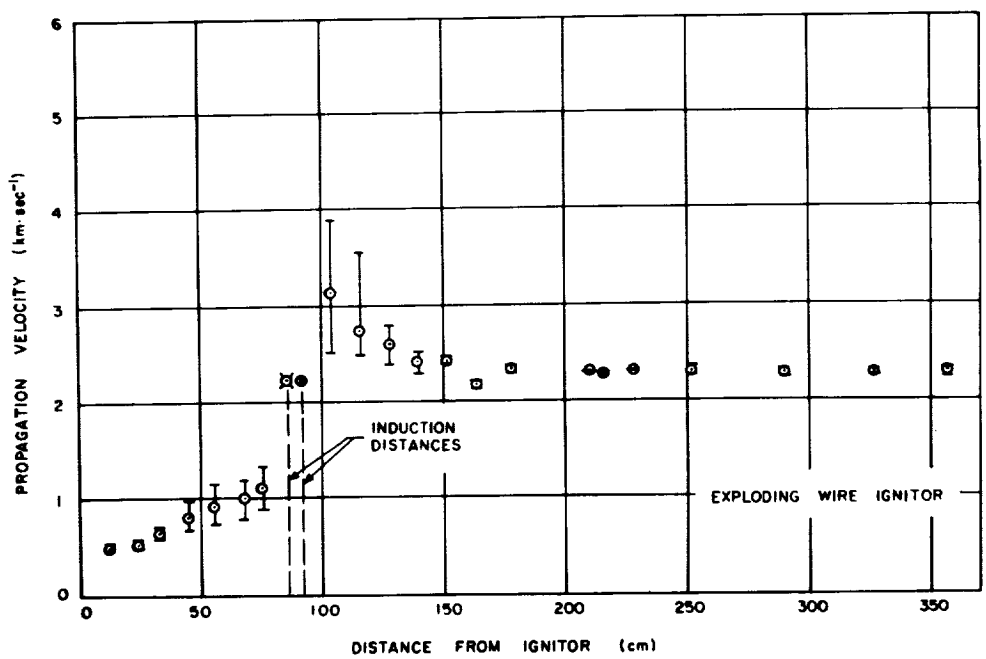

FIG. 14 RATE OF FLAME PROPAGATION IN H_2 - O_2 MIXTURE; MOLE % H_2 = 45, p_i = 5 ATM, t_i = 40°C, CLEAR TUBE.

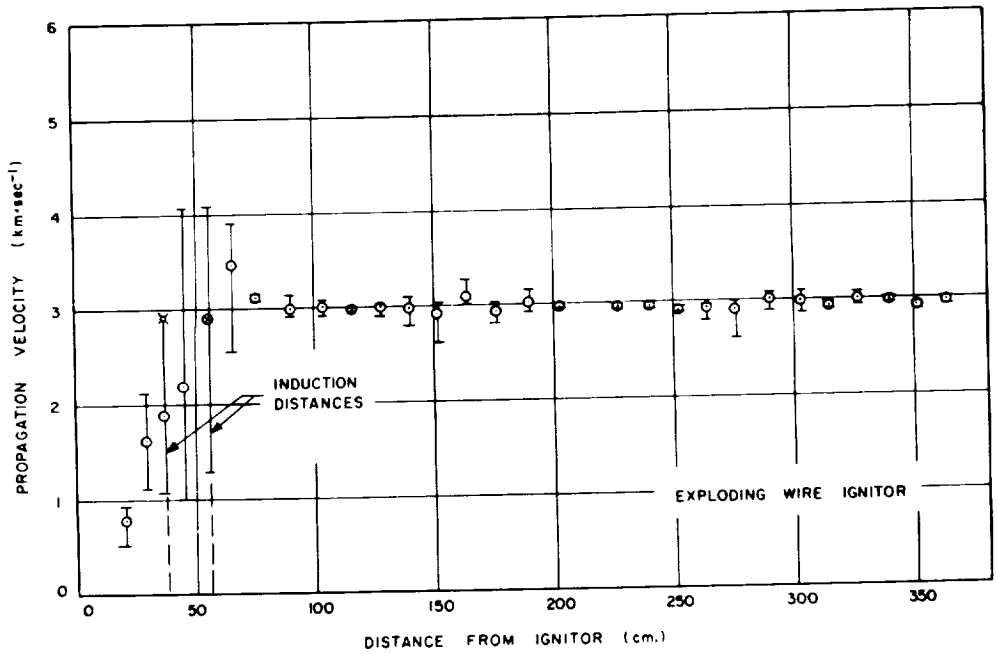

FIG. 15 RATE OF FLAME PROPAGATION IN H_2 - O_2 MIXTURE; MOLE % H_2 = 66.67, p_i = 5 ATM, t_i = 40°C, CLEAR TUBE.

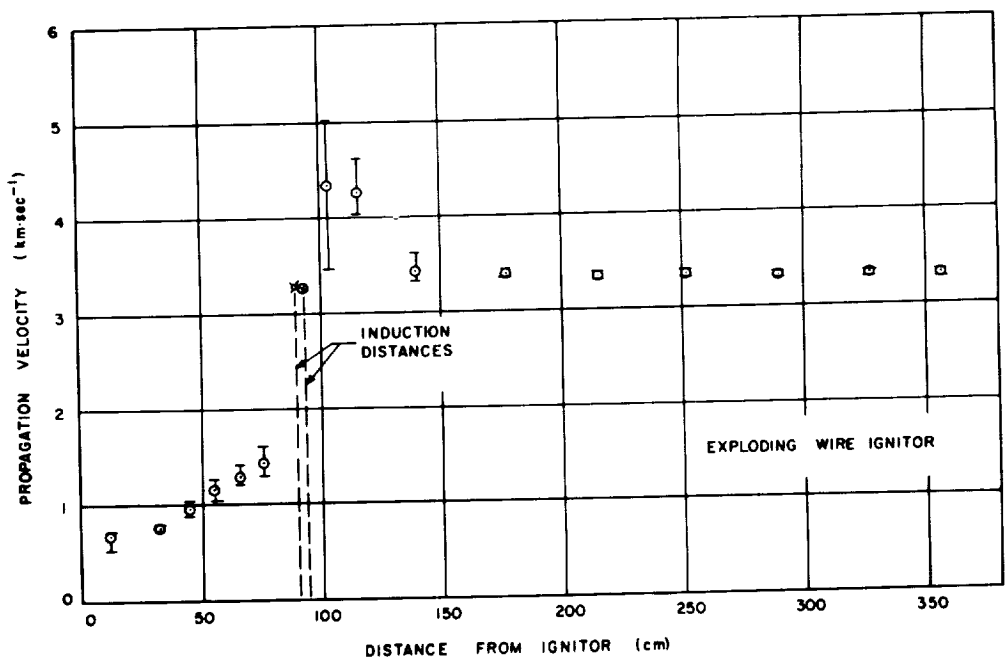

FIG. 16 RATE OF FLAME PROPAGATION IN H_2 - O_2 MIXTURE; MOLE % H_2 = 75, p_i = 5 ATM, t_i = 40°C, CLEAR TUBE.

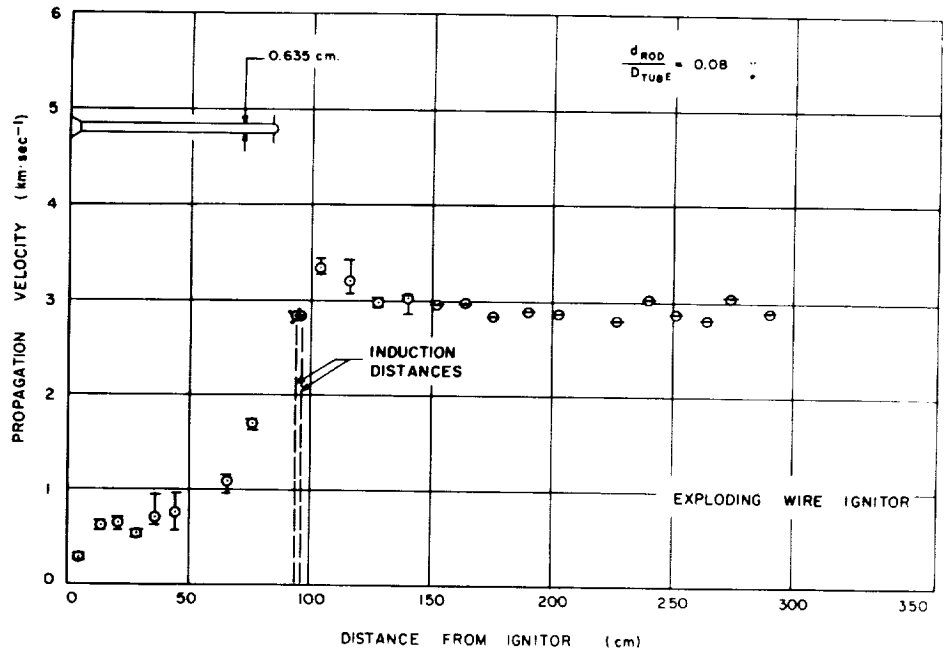

FIG. 17 RATE OF FLAME PROPAGATION IN H_2 - O_2 MIXTURE; MOLE % H_2 = 66.67, p_i = 1 ATM, t_i = 40°C, 0.635-CM DIAMETER INSERT.

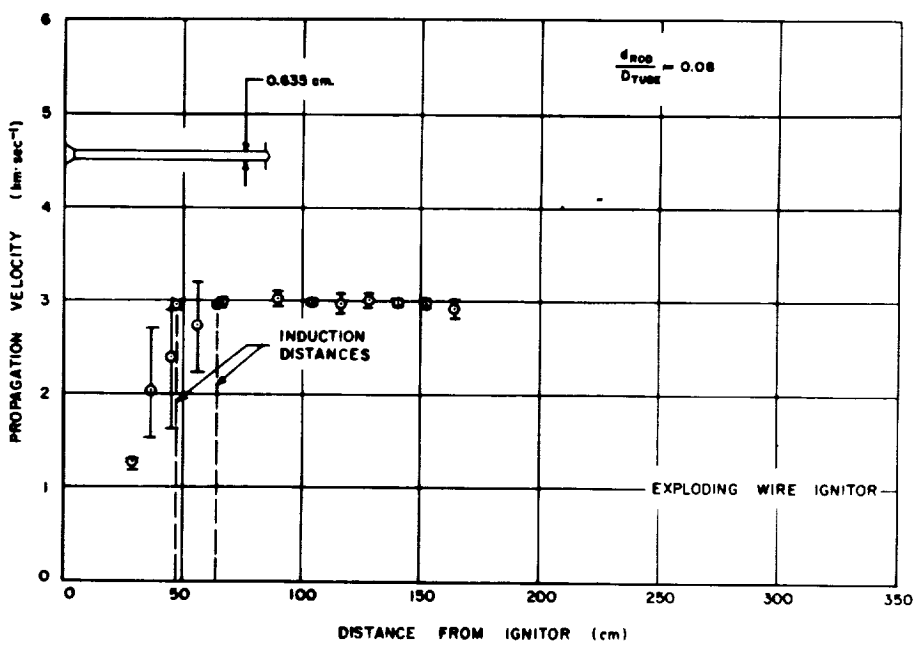

FIG. 18 RATE OF FLAME PROPAGATION IN H_2 - O_2 MIXTURE; MOLE % H_2 = 66.67, p_i = 5 ATM, t_i = 40°C, 0.635-CM DIAMETER INSERT.

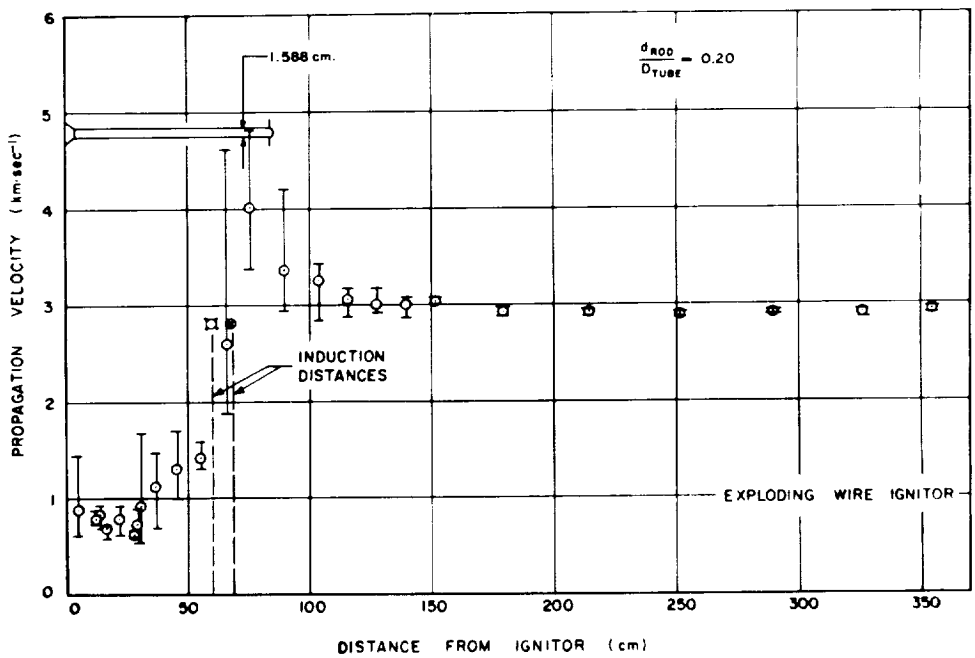

FIG. 19 RATE OF FLAME PROPAGATION IN H_2 - O_2 MIXTURE; MOLE % H_2 = 66.67, p_i = 1 ATM, t_i = 40°C, 1.588-CM DIAMETER INSERT.

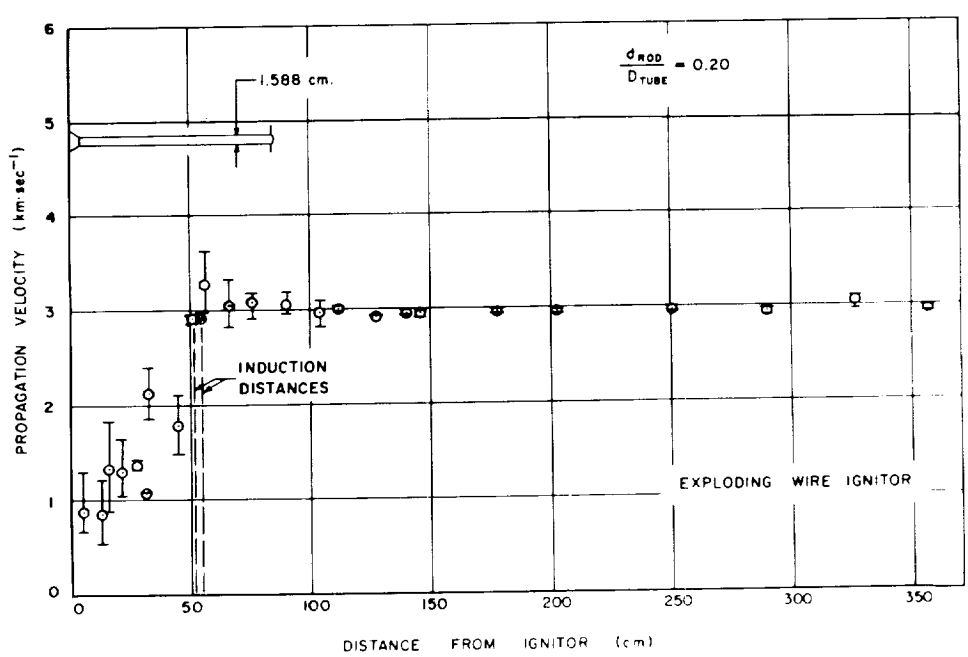

FIG. 20 RATE OF FLAME PROPAGATION IN H_2 - O_2 MIXTURE; MOLE % H_2 = 66.67, p_i = 5 ATM, t_i = 40°C, 1.588-CM DIAMETER INSERT.

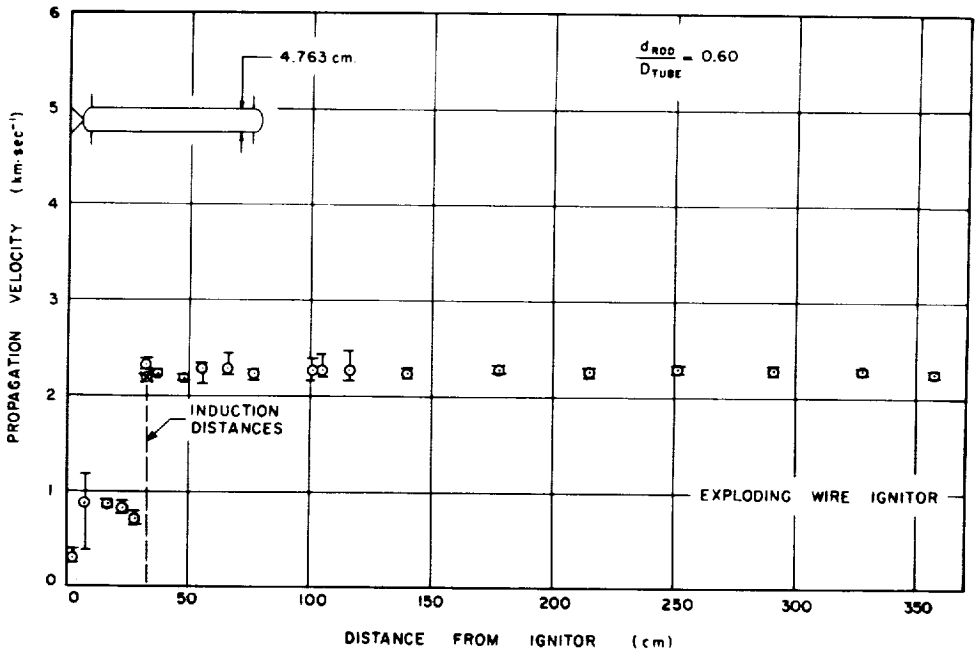

FIG. 21 RATE OF FLAME PROPAGATION IN H_2 - O_2 MIXTURE; MOLE % H_2 = 45, p_i = 1 ATM, t_i = 40°C, 4.763-CM DIAMETER INSERT.

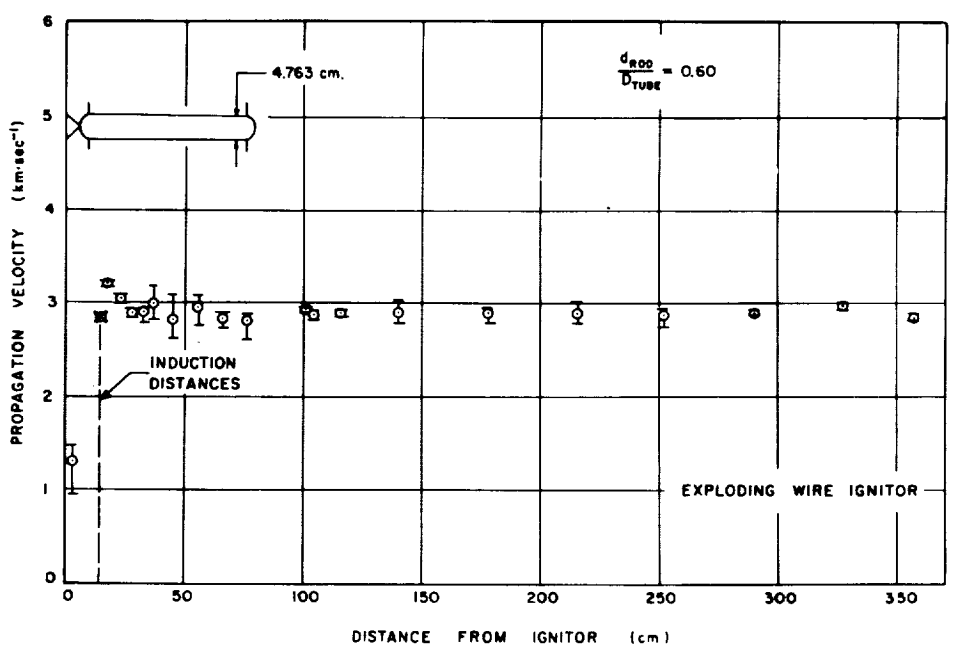

FIG. 22 RATE OF FLAME PROPAGATION IN H_2 - O_2 MIXTURE; MOLE % H_2 = 66.67, p_i = 1 ATM, t_i = 40°C, 4.763-CM DIAMETER INSERT.

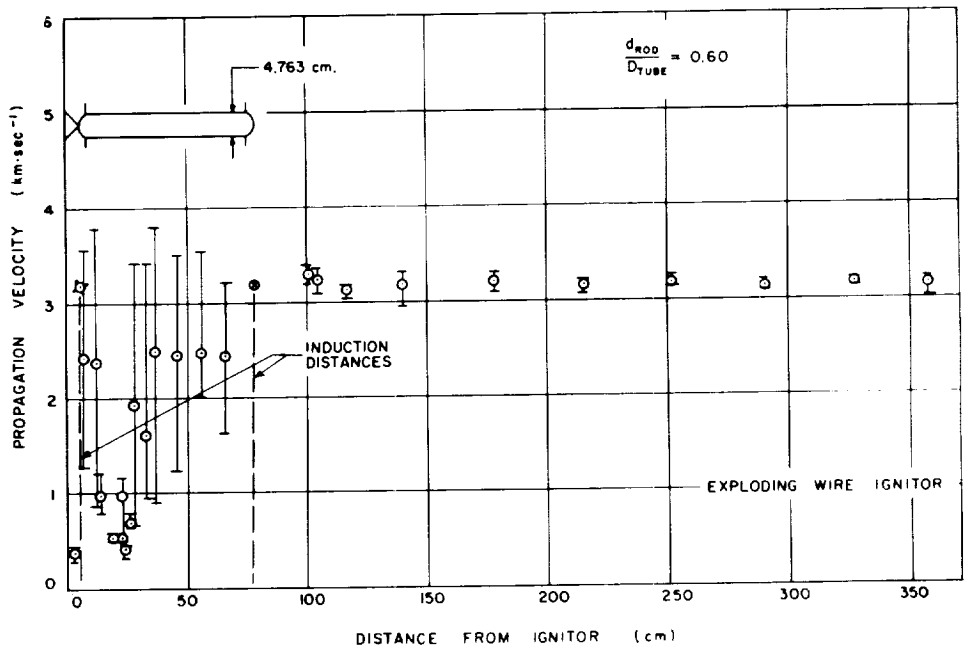

FIG. 23 RATE OF FLAME PROPAGATION IN H_2 - O_2 MIXTURE; MOLE % H_2 = 75, p_i = 1 ATM, t_i = 40°C, 4.763-CM DIAMETER INSERT.

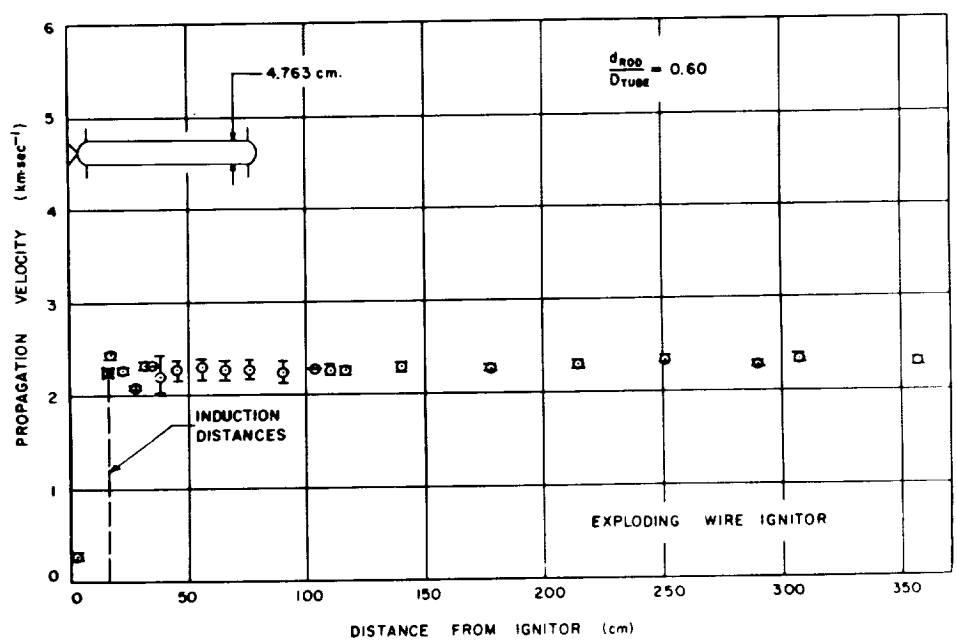

FIG. 24 RATE OF FLAME PROPAGATION IN H_2 - O_2 MIXTURE; MOLE % H_2 = 45, p_i = 5 ATM, t_i = 40°C, 4.763-CM DIAMETER INSERT.

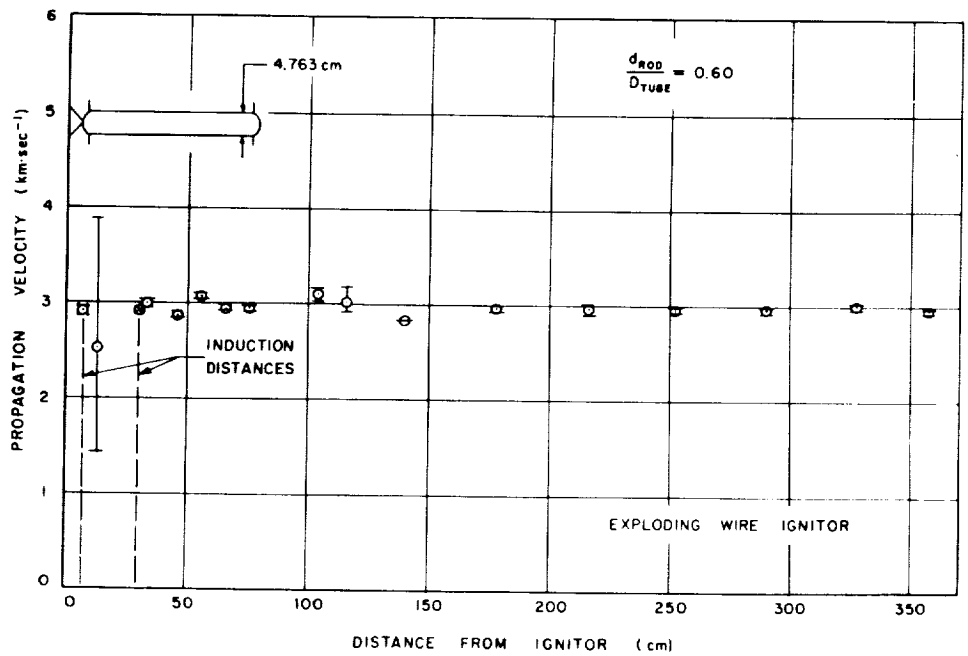

FIG. 25 RATE OF FLAME PROPAGATION IN H_2 - O_2 MIXTURE; MOLE % H_2 = 66.67, p_i = 5 ATM, t_i = 40°C, 4.763-CM DIAMETER INSERT.

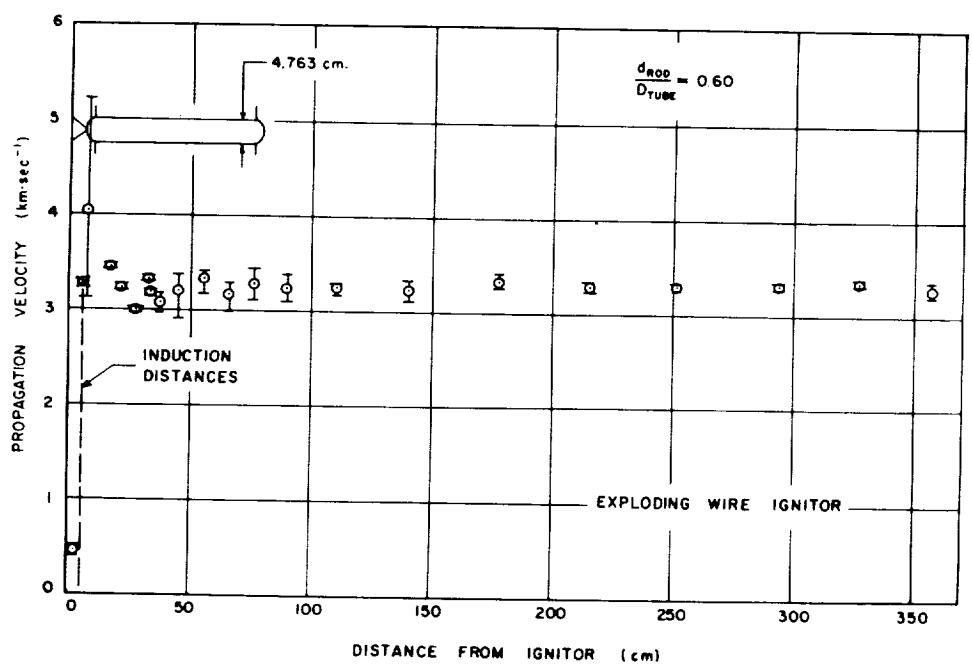

FIG. 26 RATE OF FLAME PROPAGATION IN H_2 - O_2 MIXTURE; MOLE % H_2 = 75, p_i = 5 ATM, t_i = 40°C, 4.763-CM DIAMETER INSERT.

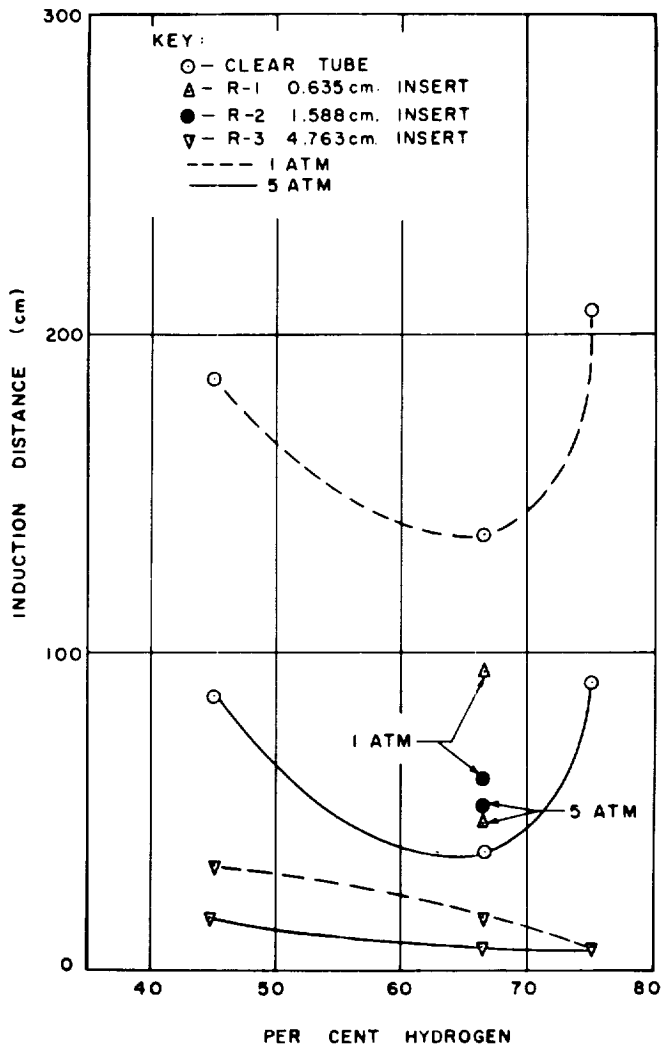

FIG. 27 DETONATION INDUCTION DISTANCES OF HYDROGEN-OXYGEN MIXTURES BASED ON MAXIMUM FLAME PROPAGATION RATES FOR THE CLEAR TUBE AND 0.635, 1.588 AND 4.763-CM DIAMETER INSERTS.

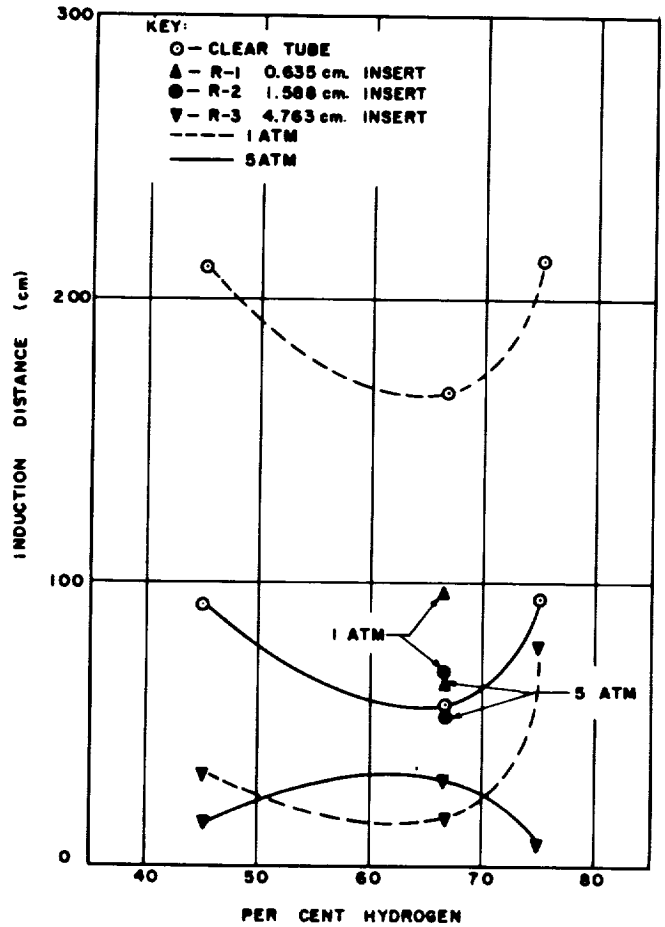

FIG. 28 DETONATION INDUCTION DISTANCES OF HYDROGEN-OXYGEN MIXTURES BASED ON AVERAGE FLAME PROPAGATION RATES FOR THE CLEAR TUBE AND 0.635, 1.588 AND 4.763-CM DIAMETER INSERTS.

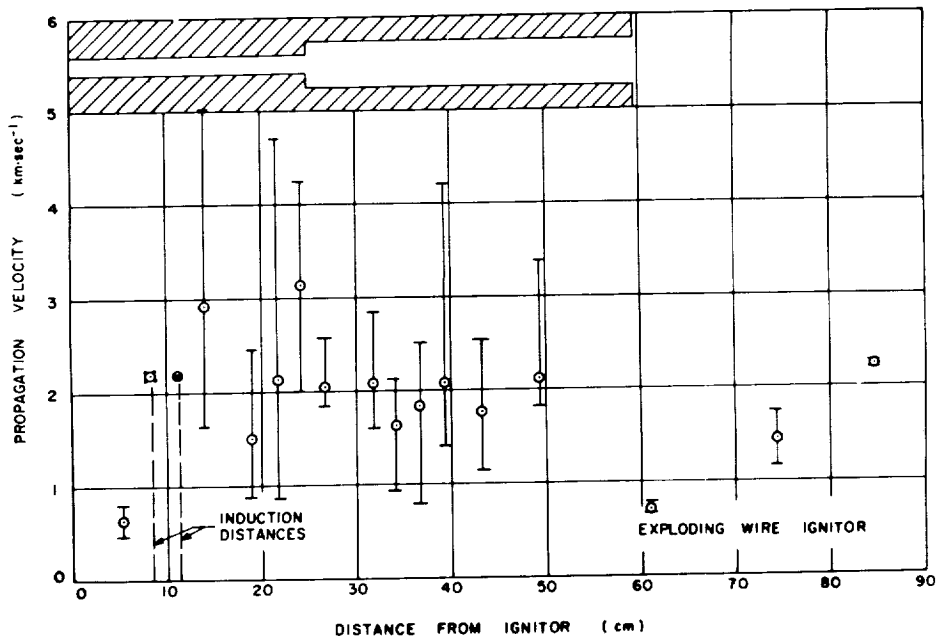

FIG. 29 RATE OF FLAME PROPAGATION IN H_2 - O_2 MIXTURE; MOLE % H_2 = 45, p_i = 1 ATM, t_i = 40°C, DIVERGENT STEPPED-WALL INSERT.

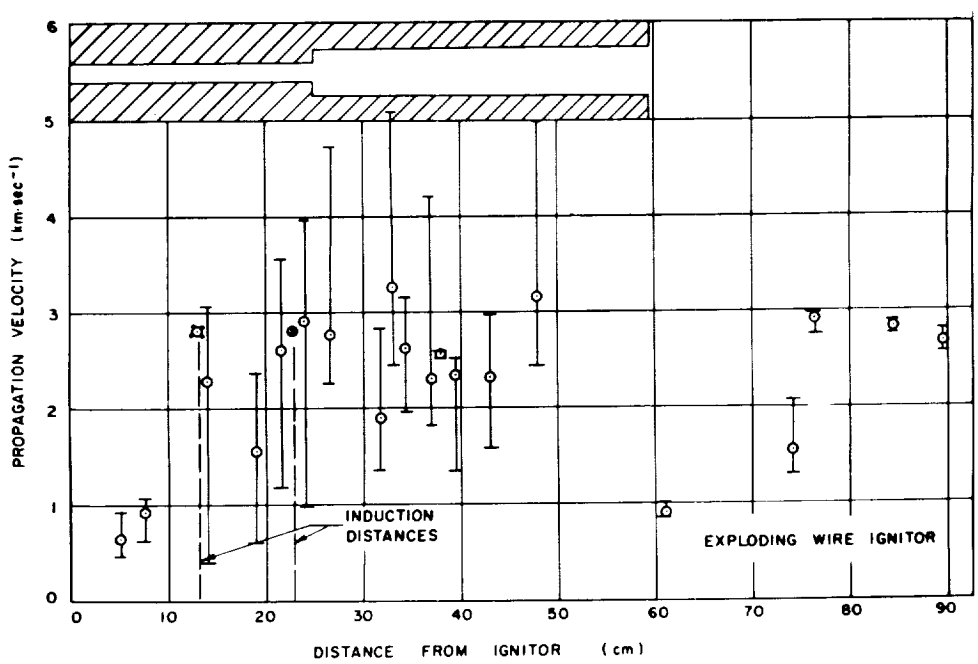

FIG. 30 RATE OF FLAME PROPAGATION IN H_2 - O_2 MIXTURE; MOLE % H_2 = 66.67, p_i = 1 ATM, t_i = 40°C, DIVERGENT STEPPED-WALL INSERT.

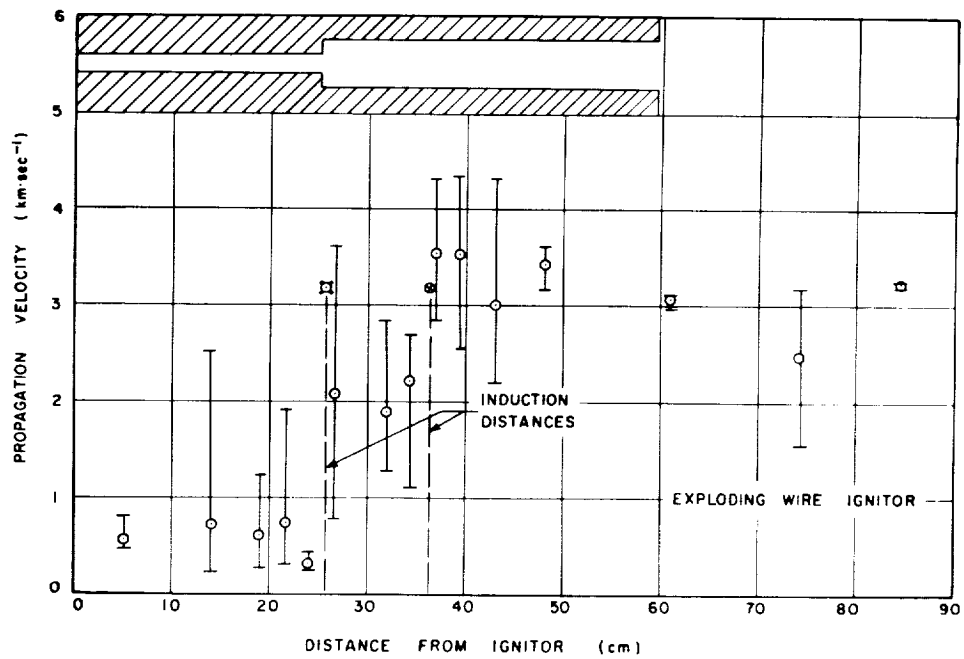

FIG. 31 RATE OF FLAME PROPAGATION IN H_2 - O_2 MIXTURE; MOLE % H_2 = 75, p_i = 1 ATM, t_i = 40°C, DIVERGENT STEPPED-WALL INSERT.

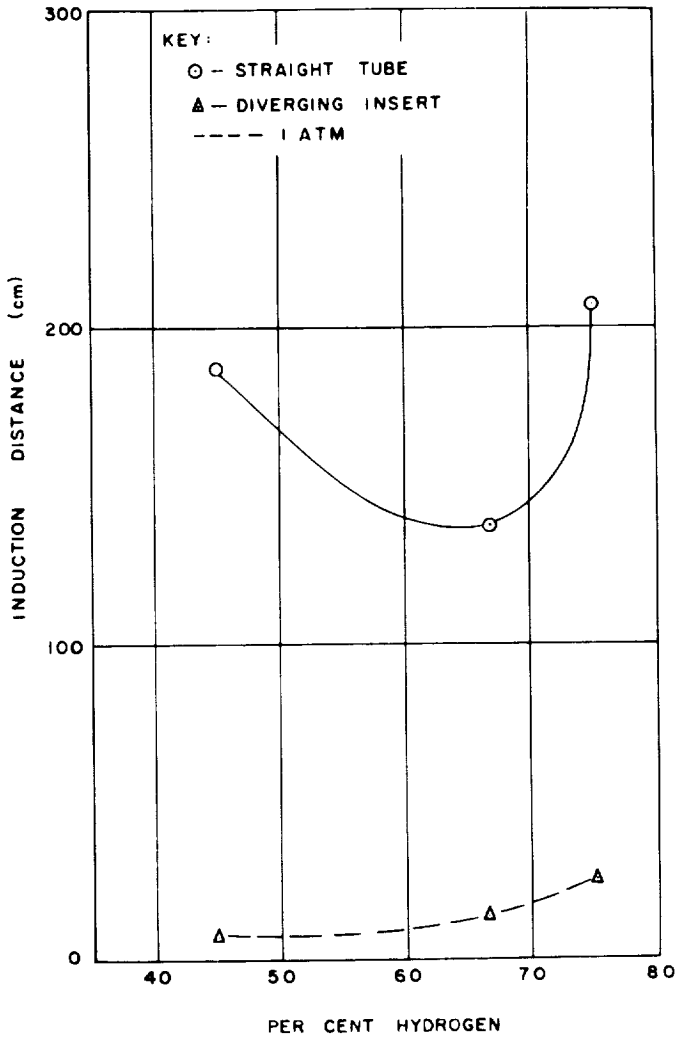

FIG. 32 DETONATION INDUCTION DISTANCES OF H_2 - O_2 MIXTURES BASED ON MAXIMUM FLAME PROPAGATION RATES WITH A DIVERGENT STEPPED-WALL INSERT.

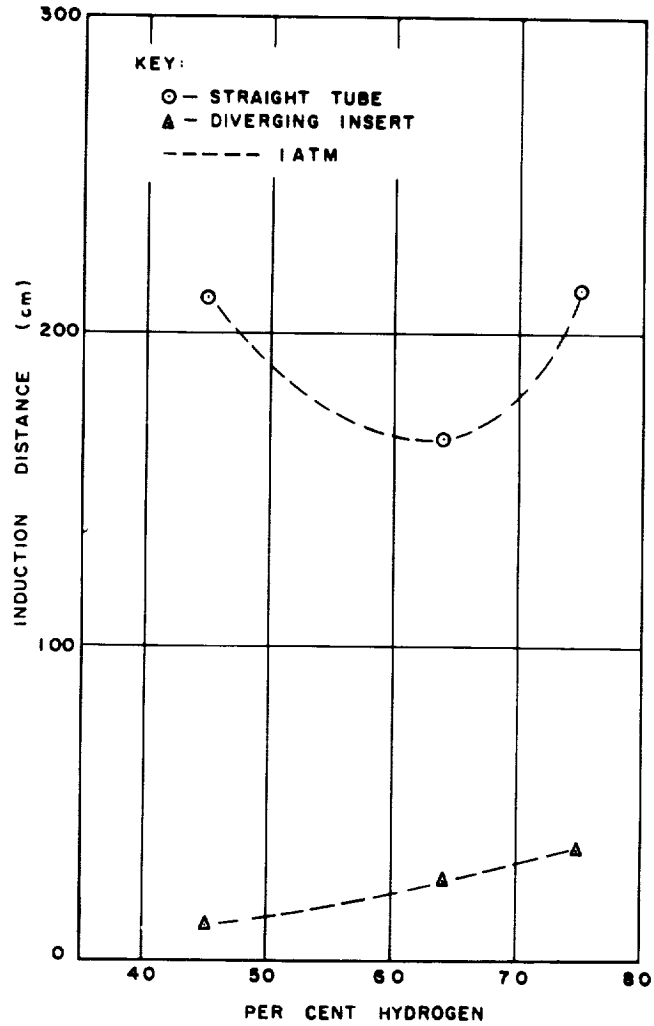

FIG. 33 DETONATION INDUCTION DISTANCES OF H_2 - O_2 MIXTURES BASED ON AVERAGE FLAME PROPAGATION RATES WITH A DIVERGENT STEPPED-WALL INSERT.

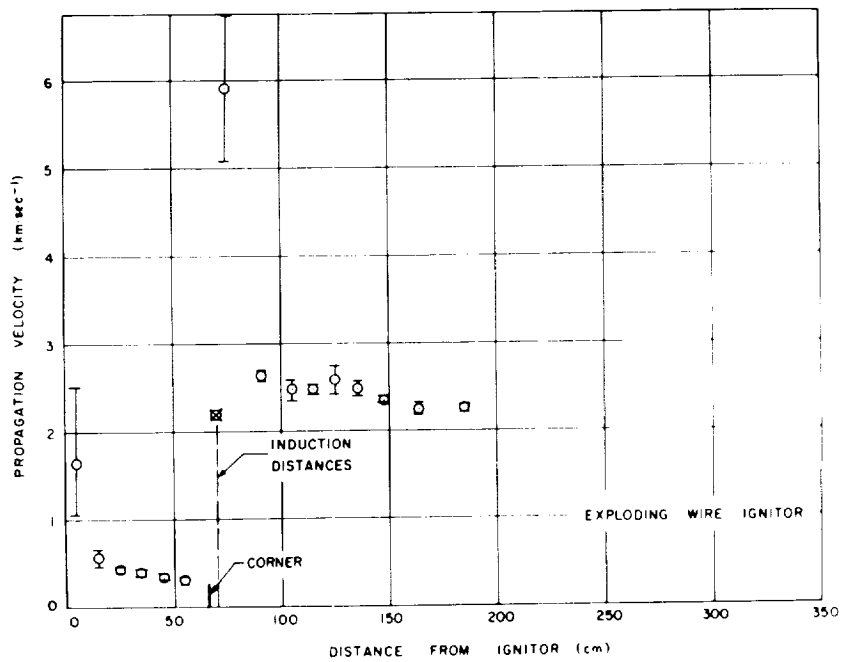

FIG. 34 RATE OF FLAME PROPAGATION IN H_2 - O_2 MIXTURE; MOLE % H_2 = 45, p_i = 1 ATM, t_i = 40°C, 90°-BEND 66 CM FROM IGNITOR.

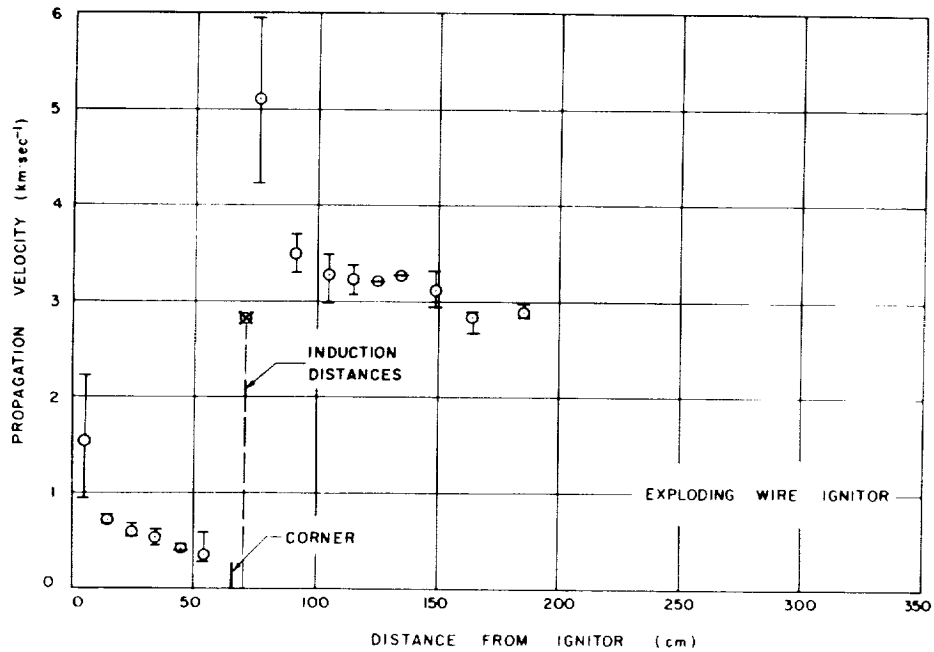

FIG. 35 RATE OF FLAME PROPAGATION IN H_2 - O_2 MIXTURE; MOLE % H_2 = 66.67, p_i = 1 ATM, t_i = 40°C, 90°-BEND 66 CM FROM IGNITOR.

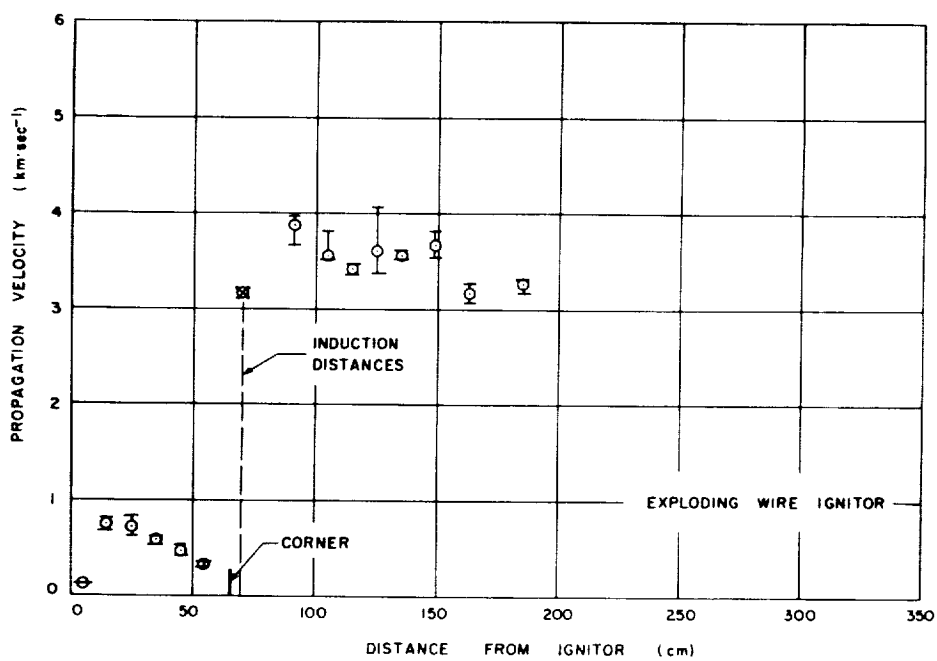

FIG. 36 RATE OF FLAME PROPAGATION IN H_2 - O_2 MIXTURE; MOLE % H_2 = 75, p_i = 1 ATM, t_i = 40°C, 90°-BEND 66 CM FROM IGNITOR.

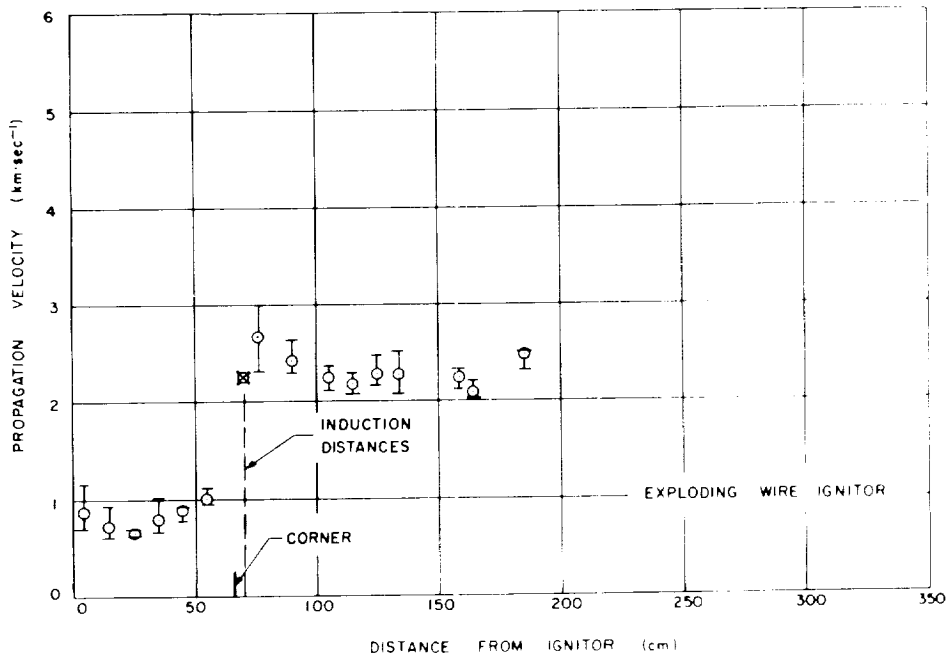

FIG. 37 RATE OF FLAME PROPAGATION IN H_2 - O_2 MIXTURE; MOLE % H_2 = 45, p_i = 5 ATM, t_i = 40°C, 90°-BEND 66 CM FROM IGNITOR.

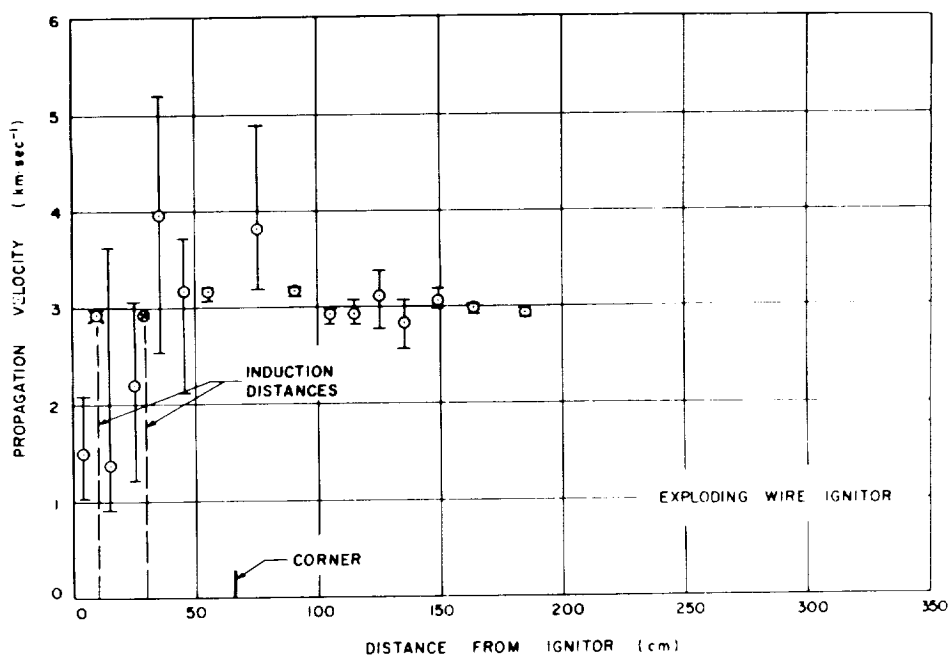

FIG. 38 RATE OF FLAME PROPAGATION IN H_2 - O_2 MIXTURE; MOLE % H_2 = 66.67, p_i = 5 ATM, t_i = 40°C, 90°-BEND 66 CM FROM IGNITOR.

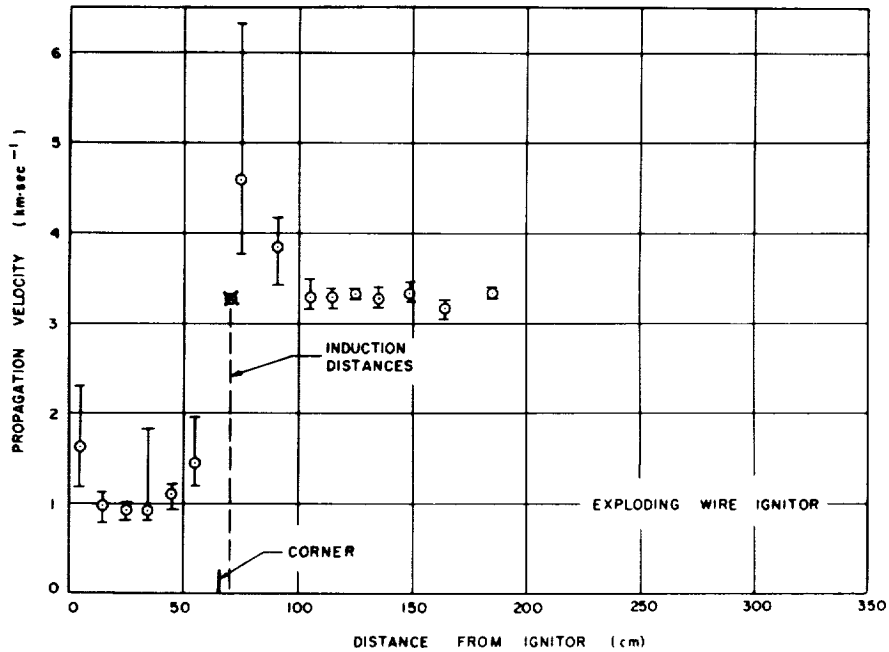

FIG. 39 RATE OF FLAME PROPAGATION IN H_2 - O_2 MIXTURE; MOLE % H_2 = 75, p_i = 5 ATM, t_i = 40°C, 90°-BEND 66 CM FROM IGNITOR.

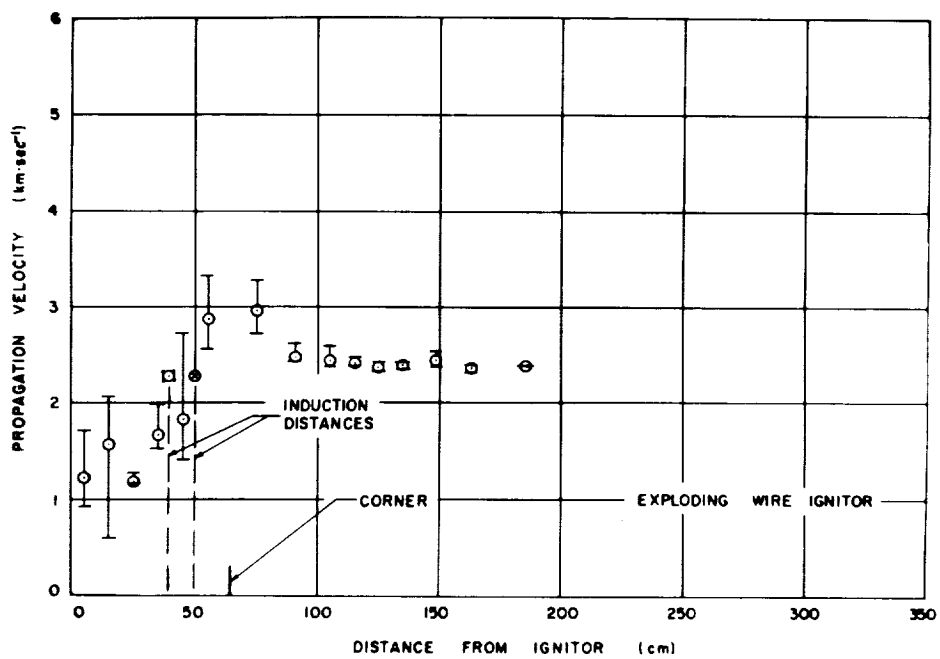

FIG. 40 RATE OF FLAME PROPAGATION IN H_2 - O_2 MIXTURE; MOLE % H_2 = 45, p_i = 10 ATM, t_i = 40°C, 90°-BEND 66 CM FROM IGNITOR.

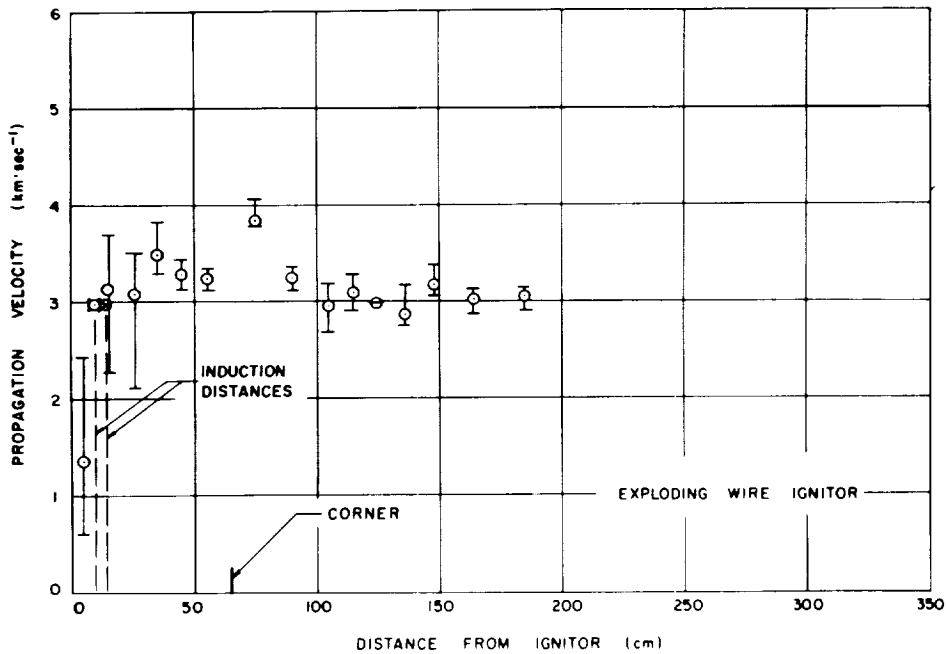

FIG. 41 RATE OF FLAME PROPAGATION IN H_2 - O_2 MIXTURE; MOLE % H_2 = 66.67, p_i = 10 ATM, t_i = 40°C, 90°-BEND 66 CM FROM IGNITOR.

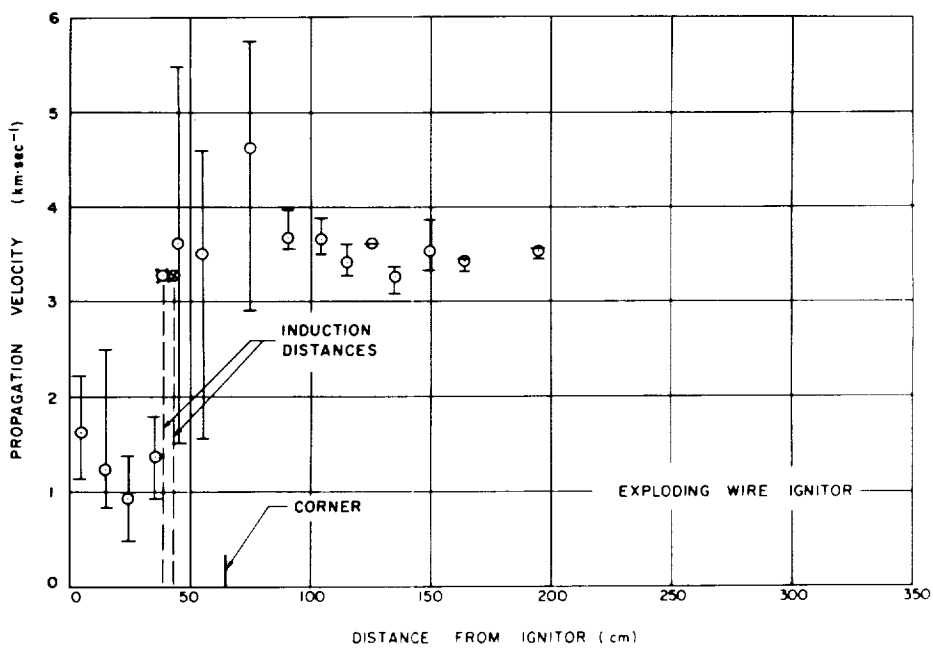

FIG. 42 RATE OF FLAME PROPAGATION IN H_2 - O_2 MIXTURE; MOLE % H_2 = 75, p_i = 10 ATM, t_i = 40°C, 90°-BEND 66 CM FROM IGNITOR.

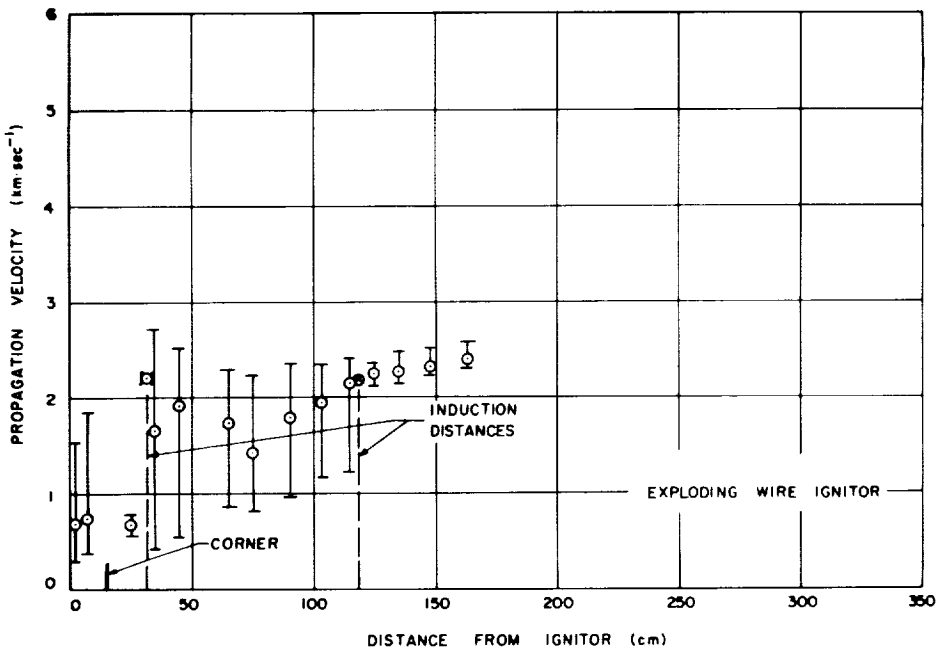

FIG. 43 RATE OF FLAME PROPAGATION IN H_2 - O_2 MIXTURE; MOLE % H_2 = 45, p_i = 1 ATM, t_i = 40°C, 90°-BEND 15 CM FROM IGNITOR.

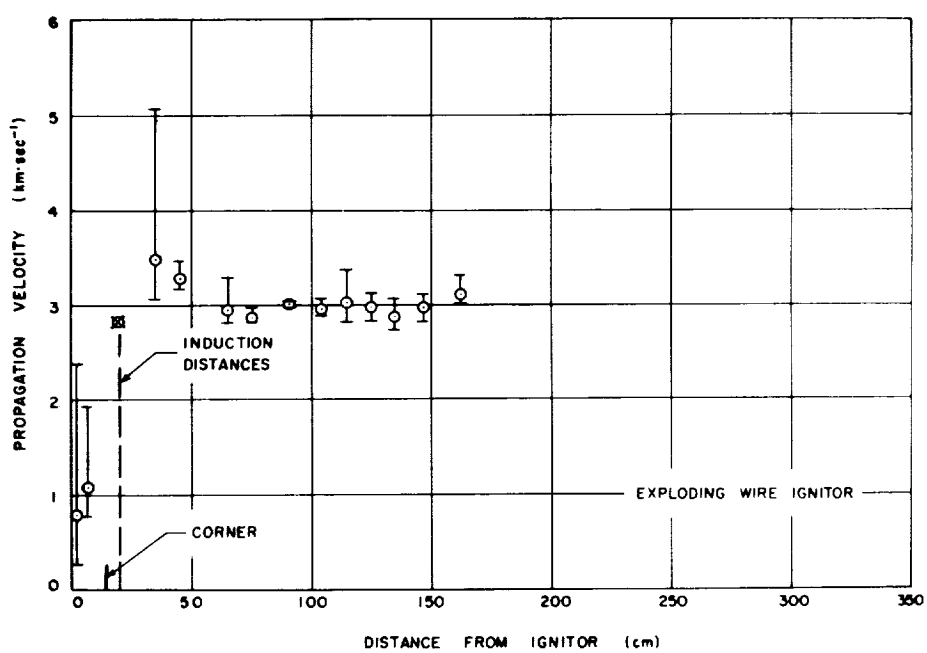

FIG. 44 RATE OF FLAME PROPAGATION IN H_2 - O_2 MIXTURE; MOLE % H_2 = 66.67, p_i = 1 ATM, t_i = 40°C, 90°-BEND 15 CM FROM IGNITOR.

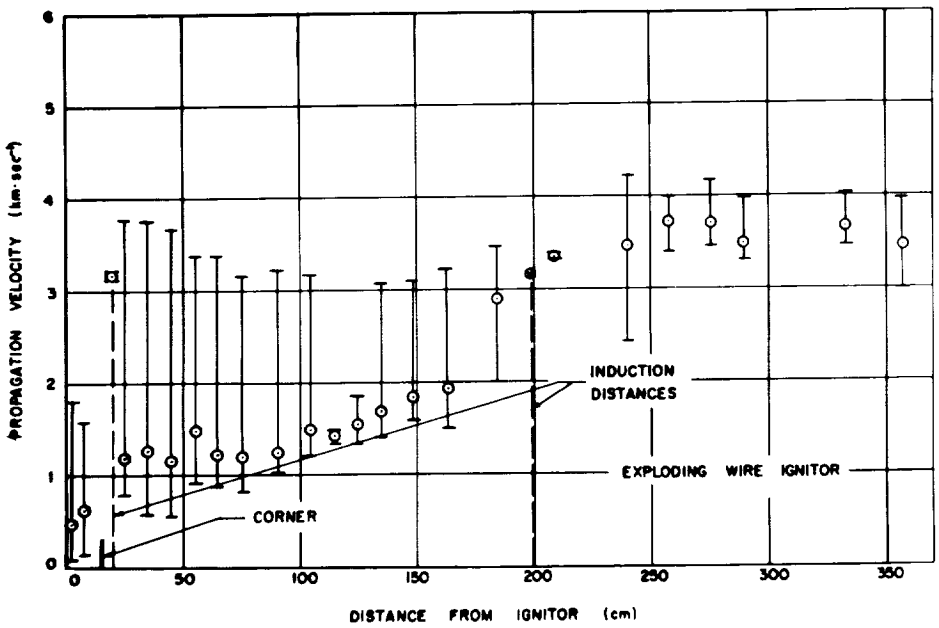

FIG. 45 RATE OF FLAME PROPAGATION IN H_2 - O_2 MIXTURE; MOLE % H_2 = 75, p_i = 1 ATM, t_i = 40°C, 90°-BEND 15 CM FROM IGNITOR.

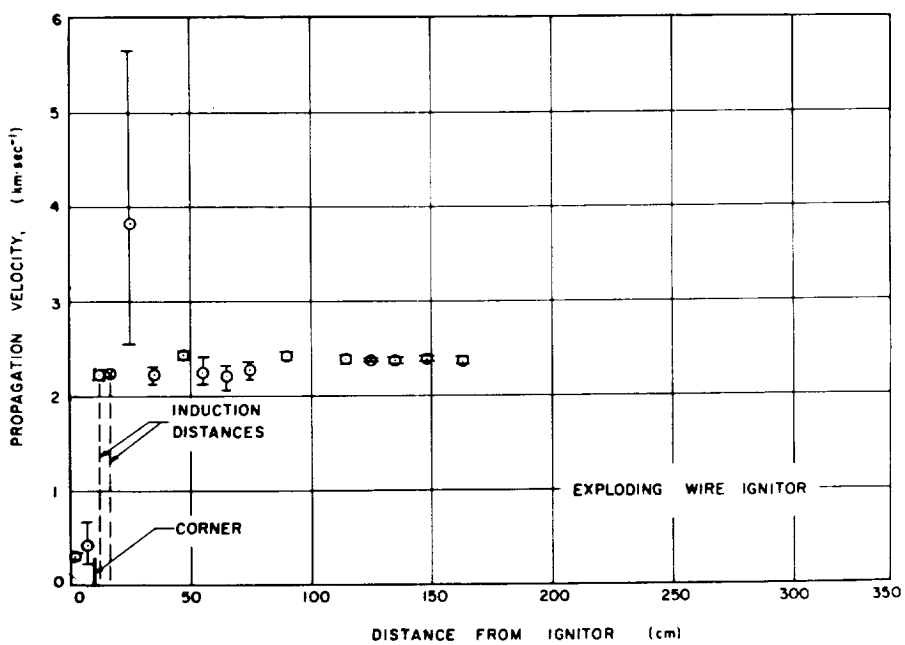

FIG. 46 RATE OF FLAME PROPAGATION IN H_2 - O_2 MIXTURE; MOLE % H_2 = 45, p_i = 5 ATM, t_i = 40°C, 90°-BEND 15 CM FROM IGNITOR.

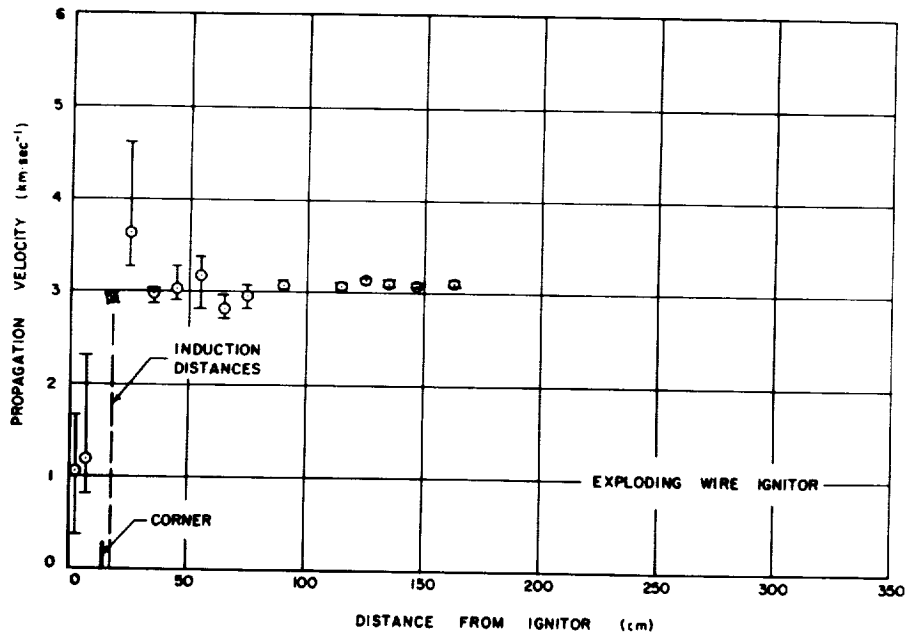

FIG. 47 RATE OF FLAME PROPAGATION IN H_2 - O_2 MIXTURE; MOLE % H_2 = 66.67, p_i = 5 ATM, t_i = 40°C, 90°-BEND 15 CM FROM IGNITOR.

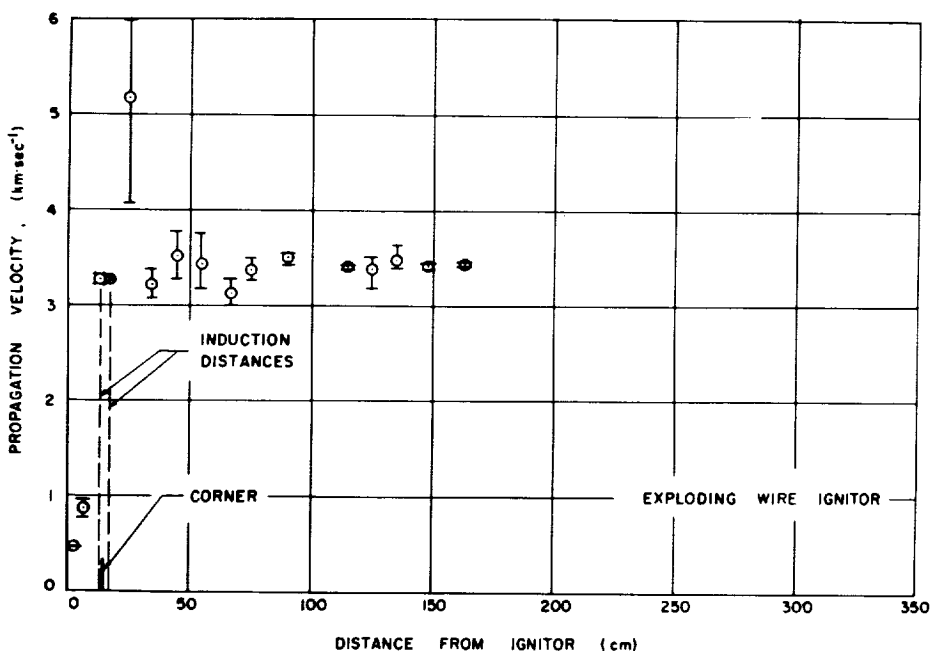

FIG. 48 RATE OF FLAME PROPAGATION IN H_2 - O_2 MIXTURE; MOLE % H_2 = 75, p_i = 5 ATM, t_i = 40°C, 90°-BEND 15 CM FROM IGNITOR.

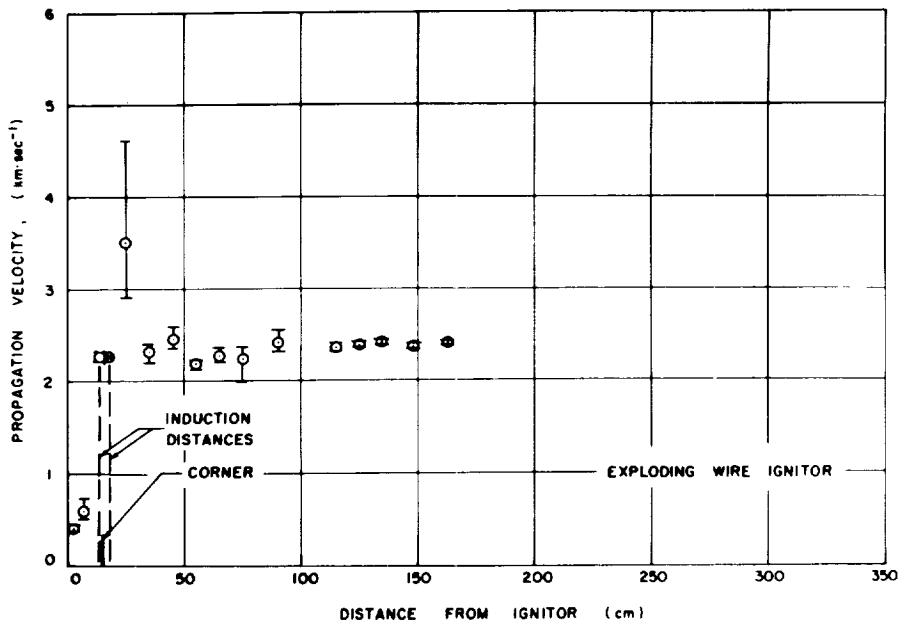

FIG. 49 RATE OF FLAME PROPAGATION IN H_2 - O_2 MIXTURE; MOLE % H_2 = 45, p_i = 10 ATM, t_i = 40°C, 90°-BEND 15 CM FROM IGNITOR.

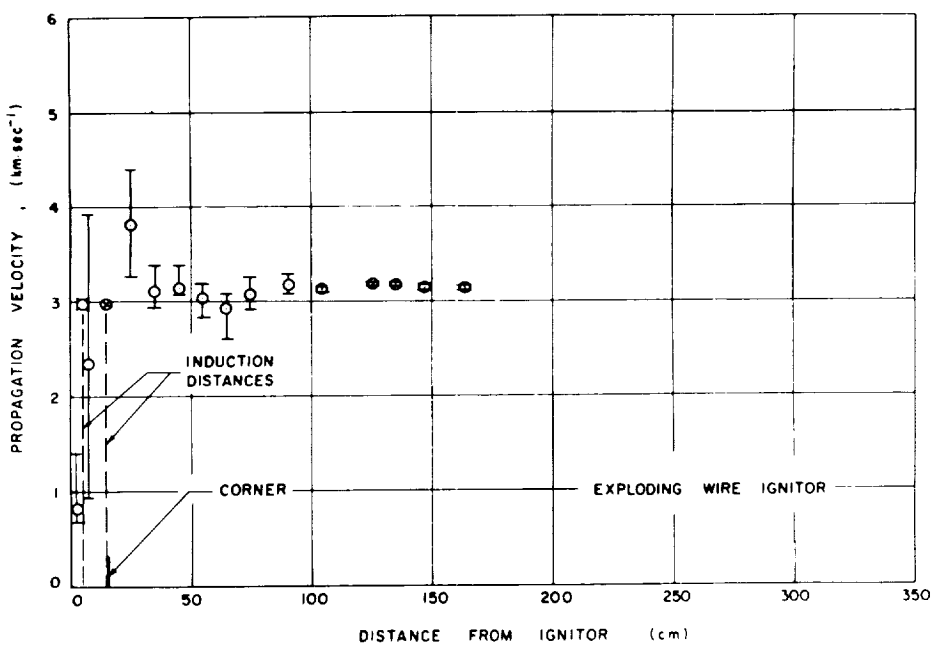

FIG. 50 RATE OF FLAME PROPAGATION IN H_2 - O_2 MIXTURE; MOLE % H_2 = 66.67, p_i = 10 ATM, t_i = 40°C, 90°-BEND 15 CM FROM IGNITOR.

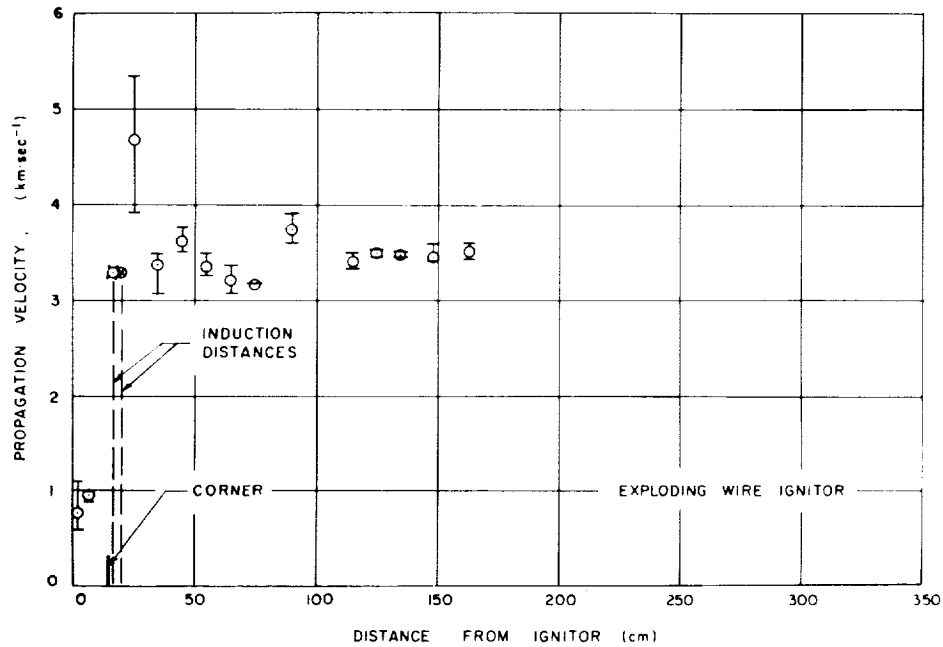

FIG. 51 RATE OF FLAME PROPAGATION IN H_2 - O_2 MIXTURE; MOLE % H_2 = 75, p_i = 10 ATM, t_i = 40°C, 90°-BEND 15 CM FROM IGNITOR.

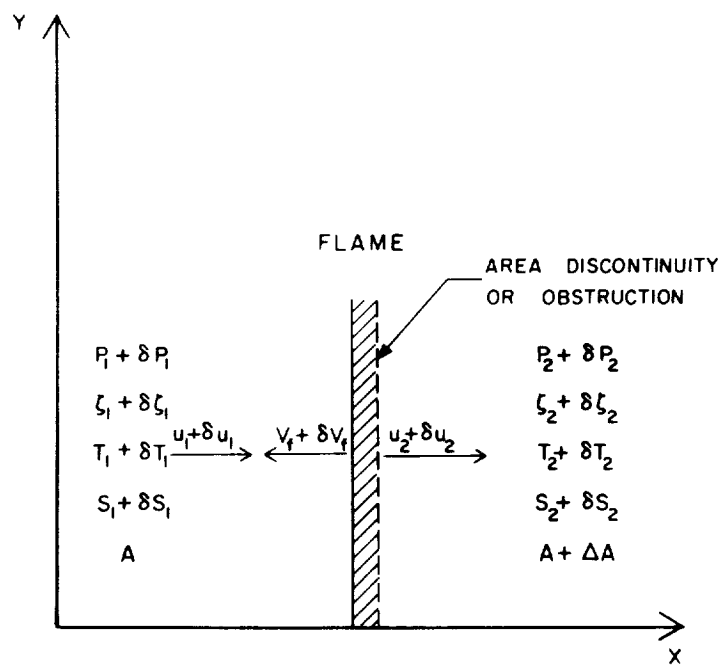

FIG. 52 COORDINATE SYSTEM ORIENTATION FOR A FLAME IN A DUCT WITH AN AREA DISCONTINUITY OR AN OBSTRUCTION.

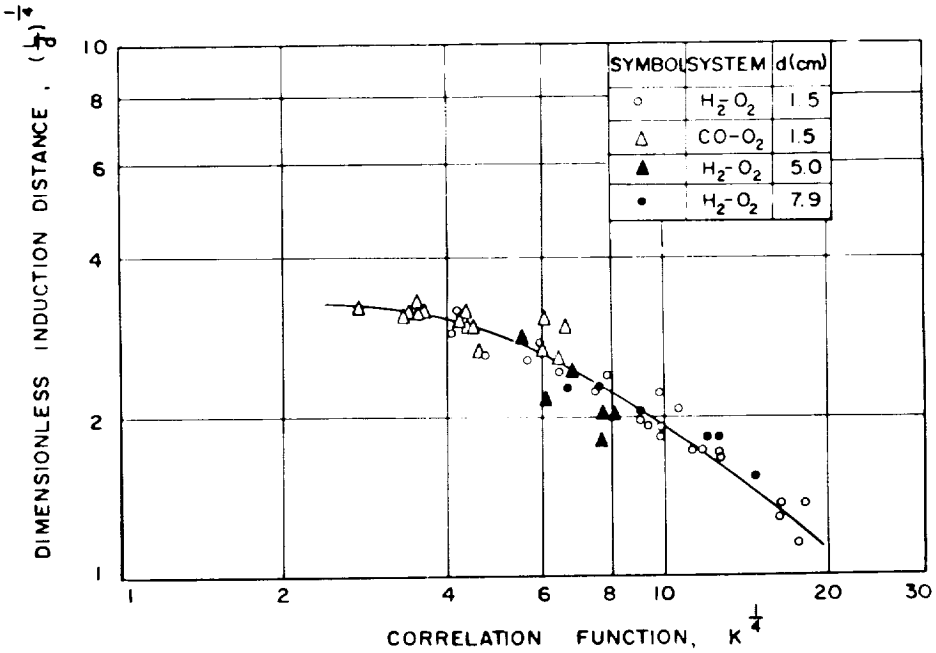

FIG. 53 DIMENSIONLESS INDUCTION DISTANCE AS A FUNCTION OF THE CORRELATION FUNCTION K.

NASA-Langley, 1963